UNIVERSITY OF BIRMINGHAM
University of Birmingham Research at Birmingham

The Cosmos greenstone succession, Agnew-Wiluna greenstone belt, Yilgarn Craton, Western Australia: Geochemistry of an enriched Neoarchaean volcanic arc succession

De Joux, A.; Thordarson, T.; Fitton, J.g.; Hastie, Alan

DOI:
10.1016/j.lithos.2014.06.013

License:
Other (please specify with Rights Statement)

Document Version
Peer reviewed version

Citation for published version (Harvard):
De Joux, A, Thordarson, T, Fitton, JG & Hastie, A 2014, 'The Cosmos greenstone succession, Agnew-Wiluna greenstone belt, Yilgarn Craton, Western Australia: Geochemistry of an enriched Neoarchaean volcanic arc succession', *Lithos*, vol. 205, pp. 148-167. https://doi.org/10.1016/j.lithos.2014.06.013

Link to publication on Research at Birmingham portal

Publisher Rights Statement:
NOTICE: this is the author's version of a work that was accepted for publication in Lithos. Changes resulting from the publishing process, such as peer review, editing, corrections, structural formatting, and other quality control mechanisms may not be reflected in this document. Changes may have been made to this work since it was submitted for publication. A definitive version was subsequently published in Lithos [VOL 205, September 2014] DOI: 10.1016/j.lithos.2014.06.013

Eligibility for repository checked October 2014

General rights
Unless a licence is specified above, all rights (including copyright and moral rights) in this document are retained by the authors and/or the copyright holders. The express permission of the copyright holder must be obtained for any use of this material other than for purposes permitted by law.

•Users may freely distribute the URL that is used to identify this publication.
•Users may download and/or print one copy of the publication from the University of Birmingham research portal for the purpose of private study or non-commercial research.
•User may use extracts from the document in line with the concept of 'fair dealing' under the Copyright, Designs and Patents Act 1988 (?)
•Users may not further distribute the material nor use it for the purposes of commercial gain.

Where a licence is displayed above, please note the terms and conditions of the licence govern your use of this document.

When citing, please reference the published version.

Take down policy
While the University of Birmingham exercises care and attention in making items available there are rare occasions when an item has been uploaded in error or has been deemed to be commercially or otherwise sensitive.

If you believe that this is the case for this document, please contact UBIRA@lists.bham.ac.uk providing details and we will remove access to the work immediately and investigate.

Download date: 25. Apr. 2024

Accepted Manuscript

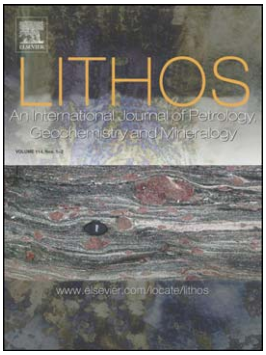

The Cosmos greenstone succession, Agnew-Wiluna greenstone belt, Yilgarn Craton, Western Australia: Geochemistry of an enriched Neoarchaean volcanic arc succession

A. de Joux, T. Thordarson, J.G. Fitton, A.R. Hastie

PII: S0024-4937(14)00219-9
DOI: doi: 10.1016/j.lithos.2014.06.013
Reference: LITHOS 3320

To appear in: *LITHOS*

Received date: 26 December 2013
Revised date: 18 June 2014
Accepted date: 19 June 2014

Please cite this article as: de Joux, A., Thordarson, T., Fitton, J.G., Hastie, A.R., The Cosmos greenstone succession, Agnew-Wiluna greenstone belt, Yilgarn Craton, Western Australia: Geochemistry of an enriched Neoarchaean volcanic arc succession, *LITHOS* (2014), doi: 10.1016/j.lithos.2014.06.013

This is a PDF file of an unedited manuscript that has been accepted for publication. As a service to our customers we are providing this early version of the manuscript. The manuscript will undergo copyediting, typesetting, and review of the resulting proof before it is published in its final form. Please note that during the production process errors may be discovered which could affect the content, and all legal disclaimers that apply to the journal pertain.

ACCEPTED MANUSCRIPT

The Cosmos greenstone succession, Agnew-Wiluna greenstone belt, Yilgarn Craton, Western Australia: Geochemistry of an enriched Neoarchaean volcanic arc succession

A. de Joux[1#], T. Thordarson[1,2], J.G.Fitton[1] and A.R. Hastie[1,3]

[1]School of GeoSciences, University of Edinburgh, Grant Institute, The King's Buildings, West Mains Road, Edinburgh, EH9 3JW, UK

[2]Faculty of Science, University of Iceland, Sturlugata 7, IS101, Reykjavik, Iceland

[3]School of Geography, Earth and Environmental Sciences, University of Birmingham, Edgbaston, Birmingham, B15 2TT

Corresponding author: alexandra_dejoux@outlook.com, +447834715146

ACCEPTED MANUSCRIPT

Abstract

The geodynamic setting of the Neoarchaean Eastern Goldfields Superterrane (EGS) of the Yilgarn Craton is the subject of debate. Some authors propose plume models, while others advocate variants on a subduction accretion model for the origin of mineralised greenstone belt sequences. Felsic volcanism in the Kalgoorlie Terrane, the western most terrane of the EGS, is considered to have a tonalite-trondhjemite-granodiorite/dacite (TTG/D) geochemical affinity. The Cosmos greenstone succession, which lies in the Agnew-Wiluna greenstone belt (AWB) of the Kalgoorlie Terrane, contains several komatiite-hosted nickel sulphide deposits, the volcanic footwall to which consists of an intercalated succession of fragmental and coherent rocks ranging in composition from basaltic andesites to rhyolites. Light rare earth elements (LREEs) and large ion-lithophile elements (LILEs) are strongly enriched relative to high field strength elements (HFSEs) across all volcanic units, and the rocks display strong

ACCEPTED MANUSCRIPT

positive Pb and negative Nb anomalies. These geochemical characteristic resemble closely those of modern high-K calc-alkaline to shoshonite continental arc successions. Contrasting rare earth element (REE), large ion lithophile element (LILE) and high field strength element (HFSE) concentrations, coupled with assimilation-fractional crystallisation (AFC) modelling, shows that the intercalated dacitic and andesitic volcanic rocks within the footwall succession are not co-genetic. Xenocrystic zircons within the felsic volcanic lithologies indicate that some assimilation of older continental crust contributed to the generation of the footwall volcanic sequence. The geochemical characteristics of the Cosmos volcanic succession indicate that parental melts were derived via partial melting of enriched peridotite that had been contaminated by subducted crustal material within the mantle wedge of a subduction zone. In contrast, two younger felsic porphyry intrusions, which cross-cut the volcanic succession, have a distinct TTG/D affinity. Therefore, these intrusions are considered to be generated via partial melting of a subducting slab and are related to local high-Ca granitoid intrusions. The Cosmos volcanic succession represents the first extrusive high-K calc-alkaline to shoshonitic volcanic arc sequence described in the Kalgoorlie Terrane and, coupled with age dating of the stratigraphy, is indicative of formation in a long-lived volcanic arc setting active from 2736 Ma to later than 2724 Ma. The composition and geochemical affinity of the volcanic footwall succession to the Cosmos komatiite-hosted nickel-sulphide deposits contrasts with the majority of felsic volcanic rocks within the AWB and also the wider Kalgoorlie Terrane, suggesting that the overall architecture of this region is more complex than is currently thought. Our conclusions not only have consequences for recent models of the tectonic evolution of the EGS but also contribute to the debate on the operation of plate tectonics during the late Archaean in general. The arc affinity of the Cosmos volcanic succession, containing abundant high-K calc-alkaline andesite lavas, provides further support for the operation of plate tectonics in the Neoarchaean.

ACCEPTED MANUSCRIPT

Keywords; Neoarchean, calc-alkaline volcanism, Kalgoorlie Terrane, subduction, island arc, Yilgarn Craton

Abbreviations

AWB – Agnew-Wiluna greenstone belt

EGS – Eastern Goldfields Superterrane

TTG/D - tonalite–trondhjemite–granodiorite/dacite

1. Introduction

Identifying the geological processes responsible for the derivation of Archaean greenstone belt sequences, such as in the Canadian Superior Craton and the Australian Yilgarn Craton, is vital for determining the possible existence of plate tectonics during the Archaean (e.g., Barnes et al., 2012; Bédard et al., 2013; Czarnota et al., 2010; Wyman, 2013). The origin of greenstone belt sequences within the Eastern Goldfields Superterrane (EGS) of the Yilgarn Craton of Western Australia (Fig. 1), which are commonly associated with komatiite-hosted nickel sulphide deposits, has been debated for over 25 years. Workers generally support either a plume-dominated model (e.g., Barnes et al., 2012; Campbell and Hill, 1988; Fiorentini et al., 2012; Trofimovs et al., 2004) or variants on a subduction accretion model (e.g., Barley et al., 2008; Czarnota et al., 2010; Gee and Swager, 2008; Kositcin et al., 2008; Nelson, 1997: 1998). Recently, Barnes et al. (2012) proposed a mantle plume model based on the composition of basalts throughout the EGS, broadly along the lines of a plume model proposed by Campbell and Hill (1988). Such plume models largely precludes the possibility of arc development and subsequent terrane accretion within the

ACCEPTED MANUSCRIPT

EGS. In contrast, Czarnota et al. (2010) provided a holistic review of the tectonic history of the EGS, which built on the work of Barley et al. (2008), and favoured a para-autochthonous convergent margin model linking all terranes of the EGS within a westward dipping subduction zone.

Understanding the tectonic setting of mineralised greenstone belt sequences has important implications both for future exploration and for understanding the geodynamics of Archaean volcanism. Geochemical analysis of individual Archaean greenstone terranes to infer a likely tectonic setting is often challenging. Within a single terrane there are often dozens of greenstone belt sequences that are, to varying degrees, poorly exposed, deeply weathered, highly metamorphosed and strongly deformed. Here we present major, trace and rare earth element (REE) geochemical data for the Neoarchaean Cosmos volcanic sequence, which lies within the Agnew-Wiluna greenstone belt in the north of the Kalgoorlie Terrane (Fig. 1) and contains several komatiite-hosted nickel sulphide ore deposits, in an attempt to resolve the relative contribution and interaction of fractional crystallisation, crustal assimilation and source composition in the formation of the Cosmos footwall volcanic succession. This data is also used here to determine its likely tectonic setting and to demonstrate that melt generation processes and tectonic evolution can be resolved even in a relatively small greenstone sequence.

2. Regional geology

The EGS comprises the eastern part of the Yilgarn Craton and features linear, bimodal (mafic–ultramafic and felsic), volcanic ‘greenstone belt’ sequences, with minor clastic sedimentary sequences and banded iron formations. These are sandwiched between voluminous elongate granitoid plutons intruded between 2760 and 2620 Ma (Fig. 1).

ACCEPTED MANUSCRIPT

SHRIMP U-Pb zircon ages indicate a major peak in volcanism between 2720 and 2650 Ma (Fig. 1), with lesser peaks at 2950 Ma and 2810 Ma (Cassidy et al., 2006; Nelson, 1997, 1998).

The Cosmos mine is situated on the western edge of the Agnew-Wiluna greenstone belt (AWB), on the north-western edge of the Kalgoorlie Terrane, which forms the western most terrane of the EGS. The AWB contains some of the world's most economically significant nickel sulphide deposits including Mount Keith, Perseverance and Yakabindie (Fig. 1). Mineralised ultramafic successions within the Kalgoorlie Terrane have a modal emplacement age of ~2707 Ma (Kositcin et al., 2008) and are commonly associated and intercalated with felsic and intermediate volcanic sequences. Examples include Black Swan (Hill et al., 2004), Perseverance (Barnes et al., 1988; Trofimovs et al., 2003), Boorara (Trofimovs et al., 2004) and Mount Keith (Fiorentini et al., 2012; Hill et al., 1995; Rosengren et al., 2008). Dacite is, volumetrically, the dominant volcanic rock type within the AWB, although lithologies range from basaltic andesites to rhyolites (Fiorentini et al., 2012; Rosengren et al., 2008). Fiorentini et al. (2012) considered the felsic volcanic rocks of AWB to compositionally exhibit a trondhjemite, tonalite and granodiorite/dacite (TTG/D) affinity. They are, thus, considered to be geochemically similar to felsic volcanic sequences in the south of the Kalgoorlie Terrane, such as the Kalgoorlie Sequence, including the Black Flag Group (Krapež and Hand, 2008; Morris and Witt, 1997) and the Boorara Domain (Trofimovs et al. 2004).

As will be demonstrated below, the footwall volcanic succession to mineralised komatiite units at Cosmos does not display a TTG/D affinity. Volcanic lithologies exhibit a distinct arc character, with a trace element geochemistry most similar to those found in modern continental subduction settings. Calc-alkaline volcanic packages, seldom described from the Kalgoorlie Terrane, are recognised within the adjacent Kurnalpi and Gindalbie Terranes of the EGS and these most likely represent the evolution and maturation of the same

ACCEPTED MANUSCRIPT

Neoarchaean volcanic arc (Fig. 1; Barley et al., 2008; Morris and Witt, 1997). However, Barnes et al. (2012) questioned whether these reported occurrences of calc-alkaline volcanism within the EGS are actually analogous to modern arc volcanism, arguing that uniformitarian models of arc accretion tectonics in the eastern Yilgarn are inconsistent with geochemical characteristics of regional basalt occurrences.

3. Geology of the Cosmos region

The Cosmos greenstone belt contains several komatiite-hosted massive and disseminated nickel-sulphide ore bodies (Fig. 2; de Joux et al., 2013; Hill and Dowling, 2008). The volcanic footwall to these ore deposits consists of a complex succession of both fragmental and coherent extrusive volcanic lithologies ranging from basaltic andesites through to rhyolites, as well as later-formed felsic and basaltic intrusions. The hangingwall consists largely of volcanically derived sedimentary rocks. The key aspects of the stratigraphy, including direct and inferred U-Pb ages, are highlighted in Table 1 and Figure 2. A level plan through the Cosmos sequence, at 200m below sea level, is given on Figure 3 and illustrates what a north-south cross-section through the primary volcanic stratigraphy may have resembled.

The Cosmos greenstone sequence has undergone several phases of regional deformation, resulting in a subvertical succession that dips and becomes younger to the east. Garnet-biotite geothermometry and metamorphic mineral assemblages indicate maximum metamorphic temperatures of ~560 - 580^{o}C at ~3 kbar (de Joux et al., 2013; Hill and Dowling, 2008). Despite experiencing amphibolite facies metamorphism and several deformation events, many of the footwall lithologies to the ultramafic lava sequences preserve primary igneous

ACCEPTED MANUSCRIPT

textures, thereby enabling protoliths to be established. A more detailed description of the stratigraphy, in particular the U-Pb dating constraints, is given by de Joux et al. (2013).

4. Sample collection and analytical techniques

104 diamond drill holes, covering ~1 km strike length of the Cosmos greenstone belt, were logged with emphasis on lithological identification of the felsic and intermediate units present within the footwall to the Cosmos Ultramafic Sequence and the underlying barren Western Ultramafic unit (Fig. 2). There is little to no surface exposure in the Cosmos North region; therefore, assessment of subsurface stratigraphy was undertaken via diamond drill core logging and sampling, thereby correlating and consolidating the stratigraphy. Lithological names were initially assigned based on textures and mineralogical assemblages of hand specimens. Subsequently, rock types were confirmed using geochemical attributes established via X-ray Fluorescence (XRF) and Inductively Coupled Plasma Mass Spectrometry (ICP-MS) in combination with petrography. Rock protolith nomenclature is used in this paper for units where primary textures are preserved or can be inferred from metamorphic mineral assemblages and/or geochemical attributes.

Core samples were crushed in a jaw-crusher and then powdered in a ring mill. These powders were used for major and trace elemental analysis. Major and trace elements were analysed on 225 samples using a PANalytical PW2402 automatic X-ray Fluorescence Spectrometer at the University of Edinburgh. Major element oxide totals were generally within +/- 2% of 100% and have been recalculated to a 100% volatile free basis. Of the samples analysed via XRF, 85 samples, which are representative of samples from each volcanic group, were analysed using ICP-MS to establish their REE concentrations, as well as selected samples for U, Th, Pb and Hf. Samples for REE analysis were prepared via tri-

ACCEPTED MANUSCRIPT

acid digest and analysed via ICP-MS at the Scottish Universities Environmental Research Centre (SUERC) in East Kilbride. Comprehensive description of XRF and ICP-MS methodology is provided in supplementary material.

5. Alteration

Element mobility during metamorphism in Archaean terranes must be considered when using major and trace element geochemistry to classify volcanic rocks and assess likely tectonic settings. Given the amphibolite metamorphic grade of the Cosmos succession, it is particularly important to be aware of the likely extent of element mobility during alteration. Post-emplacement alteration generally results in the mobility of most major elements and some large ion lithophile elements (LILE), whereas the abundances of the rare earth elements (REE), HFSE (e.g., Zr, Hf, Nb, Ta, Ti, Y), and transition metals (e.g., Ni, Cr, Co, V, Sc) are not significantly affected (Bau, 1991; Ludden et al., 1982; Winchester and Floyd, 1977; Floyd and Winchester, 1978)

The majority of major elements within different lithological groups exhibit reasonably good correlations with TiO_2, with individual volcanic units being reasonably tightly grouped (Fig. 4). The andesite lavas and dacite tuffs, however, exhibit a wider spread of data (Fig. 4). Al_2O_3 and Fe_2O_3 show typical positive correlations with TiO_2 across all lithological groups (Fig. 4b, c), implying TiO_2 generally decreases as rocks become more evolved. SiO_2 shows a negative correlation with TiO_2, with some vertical scatter within individual lithological groups, notably in the rhyolite lavas (Fig. 4a). This suggests SiO_2 may have been weakly mobile during metamorphism. Zr shows a weak negative correlation with TiO_2, although with relatively tight clustering of individual lithological groups (Fig. 4d). K_2O and Na_2O display very weak negative correlations with TiO_2, exhibiting a large scatter across the data set as a

ACCEPTED MANUSCRIPT

whole and to variable degrees within individual lithological groups. The absence of any distinct trends or patterns indicates that these elements were mobilised extensively by subsolidus metamorphic reactions (Fig. 4e, f). This mobilisation is best illustrated by the dacite lavas, which form a broad vertical array in K_2O and Na_2O space (~0.5 to ~5.5 wt. % and <0.2 to >6 wt. %, respectively) over a very narrow range in TiO_2 content (Fig. 4e, f).

When characterising the Cosmos succession, emphasis is consequently placed on those elements regarded as being least mobile during weathering, hydrothermal and regional metamorphic processes, including Th, the HFSEs and the REEs. The REE content of alteration fluids has been shown to be extremely low (e.g., Bau 1991), such that the modification of whole-rock REE patterns during diagenetic, hydrothermal or metamorphic fluid-rock interaction is minimal. The exceptions are when infiltration metasomatism is severe, fluid-rock ratios are very high, or an extensive hydrothermal system is present (e.g., Bau, 1991; Ludden et al., 1982; Michard and Albarede, 1986; Whitford et al., 1988). Selected HFSEs, used in subsequent discrimination diagrams, form relatively strong positive correlations with respect to Zr (Fig. 5a-f). On these plots individual units form relatively tight arrays, although understandably Sr shows the weakest correlation. A degree of scatter is expected, even in unaltered successions, reflecting primary spatiotemporal compositional variability within individual volcanic lithologies. REE and incompatible element compositions within the Cosmos volcanic succession are therefore considered to represent primary volcanic abundances.

The total alkali silica (TAS) plot (Le Bas et al., 1986) and the K_2O-SiO_2 subalkaline discriminatory plot (Peccerillo and Taylor, 1976; Rickwood, 1989) cannot be used to classify the Cosmos volcanic succession as the alkalis have been shown to be mobile (Fig. 4e, f). Consequently the immobile element ratio plot, Zr/TiO_2 vs. Nb/Y, of Winchester and Floyd (1977) is used to discriminate between volcanic rock types (Fig. 6). Zr/TiO_2 is used as an

ACCEPTED MANUSCRIPT

approximate measure of the degree of magmatic differentiation. Depletion in Ti becomes increasingly pronounced during continuing fractional crystallisation, whereas Zr is incompatible up until very high degrees of fractional crystallisation. Nb/Y has been shown to reflect the alkalinity of a magma series (Winchester and Floyd, 1977). The Th/Yb vs. Nb/Yb discrimination diagram of Pearce (2008), and also the Sr/Y vs. Y (Defant and Drummond, 1990; Drummond and Defant 1990) and $(La/Yb)_N$ vs. Yb_N diagrams (Martin 1986; 1999) have also been used to classify the geochemical affinity of the volcanic succession.

6. Results

The Cosmos succession comprises six main volcanic and four main intrusive lithologies, which are described in some detail below. Table 2 shows the representative chemical compositions of these lithologies.

6.1 Rhyolite lava

Rhyolite samples are tightly grouped in the corresponding field, although a few of the most metamorphosed samples have lost most of their Na_2O and gained K_2O (Figs 6, 4e and 4f). Rhyolites are enriched in LREEs with pronounced negative Eu anomalies (Eu/Eu* Average = 0.44 ($Eu_N/\sqrt{(Sm_N \times Gd_N)}$), normalised to chondrite) and have flat to slightly concave upwards HREE patterns (Gd_N/Yb_N average = 1.76, normalised to chondrite; Fig. 7a). Normal mid-ocean ridge basalt (N-MORB) normalised trace element plots show elevated LILEs (Rb, Ba, Th, U, K) and LREE relative to HFSE (Nb, Hf, Zr, Ti, Y). The rhyolite exhibits strong pronounced negative anomalies for Nb, Sr, P and Ti and a strong positive Pb anomaly (Fig. 7b).

ACCEPTED MANUSCRIPT

6.2 Dacite lavas and lapilli tuffs

Dacite lavas and lapilli tuffs compose a significant amount of the footwall to the mineralised Cosmos Ultramafic Sequence (Figs. 2, 3). Their common mineralogy, overlapping U-Pb ages (Table 1; Fig. 2), and intercalation with andesite lavas (Fig. 3) suggest they are genetically related and represent the effusive and explosive components respectively of the same magma source (de Joux et al., 2013). Geochemically they are also very similar (Fig. 7c-f). However, while dacite lavas are tightly grouped on Figures 4, 5 and 6, the dacite lapilli tuffs show a wider scatter. This is not surprising given the fragmental nature of the dacite lapilli tuffs, comprising volcanic fragments that have been subsequently metamorphosed. Both the dacite lapilli tuffs and the lavas show highly variable Na_2O and K_2O contents (Fig. 4a, e, f) reflecting the latter elements mobilities during metamorphism (i.e. the degree of albitisation versus sericitisation). Elevated SiO_2 in the rocks is likely an artefact of Si immobility during metamorphism (rather than addition of Si into the system) and implies that there is a net loss of other elements, such as Na and K, during this process. Both the lavas and tuffs show enriched LREE patterns and exhibit nearly flat HREE patterns (Gd_N/Yb_N average lava = 1.95, Gd_N/Yb_N average tuff = 1.77; Fig. 7c, e). Moderate negative Eu anomalies are present in both lavas (Eu/Eu* average = 0.71) and tuffs (Eu/Eu* average = 0.72), but are less pronounced than those exhibited by rhyolites (Fig. 7c, e). N-MORB-normalised trace element plots for both lavas and tuffs are very similar (Fig. 7d, f), each showing elevated LREE and LILEs relative to HFSEs with pronounced negative anomalies for Nb, Sr, P and Ti, and a strong positive anomaly for Pb. These anomalies are less pronounced than those within the rhyolite samples.

ACCEPTED MANUSCRIPT

6.3 Garnet-hornblende felsic schist

Poor primary textural preservation within this unit renders protolith assignment difficult. The primary mineralogy has been almost entirely overprinted by abundant garnet porphyroblasts in a strongly banded hornblende-plagioclase matrix (Table 1). Garnet abundance, size and occurrence is highly variable throughout the unit, as is the proportion of mafic and felsic domains. This variation is seen in the SiO_2, which varies between 56 and 71 wt. %, giving the unit a broadly andesitic/dacitic composition. However, the data is tightly grouped in the rhyodacite-dacite field of Figure 6, suggesting that this variability in silica is largely controlled by removal or addition of elements during recrystallisation metamorphism. Despite these large variations in major element concentrations (e.g., SiO_2 ~56 to 70 wt. %) the schist features remarkably constant REE compositions (Fig. 7g), with relatively enriched LREEs, flat HREE patterns (Gd_N/Yb_N average = 1.43) and a negative Eu anomaly (Eu/Eu* average = 0.71) (Fig. 7g). The chondrite- and N-MORB-normalised diagrams show that the schist has a similar composition to the dacite lavas and dacitic lapilli tuffs, with notable enrichment in LILEs and the LREE, strong negative anomalies for Nb, Sr, P, and Ti, and a strong positive Pb anomaly (Fig. 7h). This suggests a volcaniclastic deposit with dacite composition as the most likely protolith.

6.4 Andesites and associated volcaniclastic units

Despite their relatively constant Nb/Y, intermediate lavas and associated volcaniclastic rocks range from basaltic andesites to andesites, although the majority of points plot in the andesite field (Fig. 6). In comparison to the felsic volcanic rocks, these andesite lavas are less LREE-rich with flatter HREE trends (Gd_N/Yb_N average = 1.57) and no

ACCEPTED MANUSCRIPT

appreciable Eu anomaly (Eu/Eu* average = 0.93; Fig. 7i). Multi-element plots also show less enrichment in LILEs and a lack of the distinct anomalies seen within the dacite and rhyolite units, although negative Nb and positive Pb anomalies are distinct and there are small negative Ti and P anomalies (Fig. 7j).

6.5 Intermediate crystal tuff

This unit is andesitic in composition with tight grouping of the data in the andesite compositional field on Figure 6. It is compositionally similar to the overlying younger andesite lavas. This unit is the least LREE-rich of all the Cosmos footwall volcanic rock units, exhibits a small negative Eu anomaly (Eu/Eu* average = 0.81) and has a flat HREE pattern (Gd_N/Yb_N average = 1.49; Fig. 7k). N-MORB-normalised plots are very similar to those of the andesites and show a strong positive Pb anomaly and less pronounced negative Nb and Ti anomalies (Fig. 7l).

6.6 Mafic intrusions

Multiple mafic intrusions crosscut the Cosmos volcanic succession. The two largest of these are the Cosmos Deeps and AM5 mafic intrusions, which intrude largely parallel to the subvertical stratigraphical boundaries (Fig. 2). The morphology and extent of the AM5 intrusion is poorly constrained due to drilling paucity. These two main intrusions are compositionally distinct, forming discrete clusters on Figure 6. The Cosmos Deeps intrusion is a dolerite, while the AM5 intrusion is slightly more evolved or a diorite. The REE patterns are poorly fractionated, with flat HREE patterns and slight positive Eu anomalies (Eu/Eu*

ACCEPTED MANUSCRIPT

average = 1.16). The Cosmos Deeps dolerite is more enriched in LREEs and has a steeper HREE pattern (Gd_N/Yb_N average = 1.76) than the AM5 diorite (Gd_N/Yb_N average = 1.10), but neither intrusion displays the level of enrichment in LREEs seen within the majority of extrusive volcanic units (Fig. 7m). The intrusions show enrichment in Rb and Ba but depletion in Th and U compared to the extrusive volcanic units. Both intrusions have negative Nb anomalies and positive Pb anomalies (Fig. 7n). HFSE patterns are generally flat with the AM5 diorite having only a weak P anomaly. The Cosmos Deeps dolerite has distinct negative Hf and Zr anomalies (Fig. 7n).

6.7 Felsic porphyry intrusions

Two felsic porphyry intrusions crosscut the volcanic succession. They differ in age and mineralogy, with the older hangingwall intrusion dated at ~2670 Ma while the younger footwall intrusion is dated at ~2653 Ma. Thus, the footwall and hangingwall felsic porphyries are respectively ~71 Ma and ~54 Ma younger than the youngest age of 2724 Ma obtained for the volcanic footwall volcanic sequence (Fig. 2; de Joux et al., 2013). Despite their age difference, the two intrusions are geochemically similar, with high Al_2O_3 (over ~15 wt. %; Fig. 4b), high Sr (~350 - 550 ppm; Table 3) and low Y concentrations (<5 ppm; Fig. 5c; Table 3). They are geochemically similar to each other, with REE concentrations that are strongly fractionated (Gd_N/Yb_N average = 5.09) compared to those of the Cosmos extrusive volcanic lithologies. Eu anomaly (Eu/Eu* average = 1.01) is absent from both intrusions, which also are LREE-rich but strongly depleted in HREEs, with HREE concentrations in the older footwall intrusion approaching chondrite values between Ho and Lu (Fig. 7o). They are LILE-rich and exhibit large negative Nb and positive Pb anomalies (Fig. 7p). Their composition is also typified by steeply dipping multi-element plots with HFSEs and HREEs strongly depleted with respect to N-MORB (Fig. 7o, p).

ACCEPTED MANUSCRIPT

7. Discussion

7.1 Trends in trace and rare earth element geochemistry

All extrusive volcanic units exhibit LREE and LILE enrichment compared to HREEs and HFSEs. Multi-element plots show strong negative anomalies for Nb, Sr, P, Eu and Ti within the rhyolites, dacite lavas and lapilli tuffs, and the garnet-hornblende schist (Fig. 7). Low overall Ti, Sr, P and Eu abundances with respect to their adjacent elements and N-MORB are indicative of restite phases in the source region or fractional crystallisation involving phases in which these elements are compatible, or a combination of these processes. Negative Eu anomalies are typical of melts separated from residues containing feldspar, which is the major host of Eu^{2+}, either in the source region or during later plagioclase fractionation. The negative Sr anomaly is also controlled by residual plagioclase in the source region or by plagioclase fractional crystallisation. Negative Ti anomalies are likely to be related to crystallisation of a Ti-bearing oxide, such as magnetite or titanite. The amplitude of the Ti anomalies increases as the units become more evolved, reflecting the increasing abundance of Ti-bearing phases in the crystallising assemblages as fractional crystallisation proceeds. The large negative P anomalies are controlled by residual apatite in the source region and/or its presence during fractional crystallisation.

The intermediate volcanic units are less LILE-rich than the felsic units (Fig. 7). They also lack the distinct negative anomalies seen in the dacite and rhyolite lithologies, notably a significant negative Eu anomaly, although both the andesite lavas and intermediate crystal tuff have small negative Ti and Sr anomalies.

On Figure 6 the Cosmos dolerite and AM5 diorite form two distinct clusters and plot away from the andesite lavas. The AM5 diorite lacks the appreciable LREE enrichment seen

ACCEPTED MANUSCRIPT

in the andesite lavas and thus is unlikely to be a sub-volcanic expression of the andesite volcanism. The Cosmos Deeps dolerite is the only unit with distinct negative Hf and Zr anomalies. The contrasting trace element characteristics show that the two intrusions are not genetically related.

The two felsic intrusions have incompatible element concentrations that are distinct from those of the Cosmos extrusive volcanic succession (Fig. 5b, c, e) and have depleted HREE concentrations. These characteristics, along with average Sr > 420ppm, Y < 5ppm and no perceptible Eu anomaly, indicate that they have a strong TTG/D affinity (Table 3). REEs in TTG/Ds are strongly fractionated; the average $(La/Yb)_N$ of the footwall and hangingwall intrusions is ~70 and ~54 respectively compared with the TTG/D average $(La/Yb)_N$ of ~ 38 (Martin, 1994).

Negative Nb and positive Pb anomalies are prominent in all extrusive and intrusive lithological groups. These anomalies are characteristic of modern subduction-related calc-alkaline magmas and the continental crust.

7.2 Crustal signature displayed by the Cosmos volcanic sequence

The Cosmos volcanic footwall sequence displays a strong crustal signature as indicated by the overall enrichment in LILEs and LREEs, relative to N-MORB and chondrite respectively, as well as strong positive Pb and negative Nb anomalies. Trace and REE geochemistry indicates that parental melts were most likely generated via partial melting of metasomatised mantle, a process that commonly occurs in modern subduction zones. Crustal material from subducted sediments and oceanic crust are transferred by either dehydration or melting to the overlying mantle wedge (Johnson and Plank, 1999; Pearce and Peate, 1995). LILEs and LREEs are preferentially partitioned into hydrous fluids during dehydration of the

ACCEPTED MANUSCRIPT

subducting slab, thereby enriching partial melts of peridotite formed in the overlying mantle wedge. HFSEs are conservative (not mobilised) during slab dehydration and, thus, are not enriched in the mantle wedge relative to N-MORB source regions (Pearce and Peate, 1995). Addition of crustal material from melting of subducted sediment may also enrich the mantle wedge. The absence of depleted HREE signatures in all these units, except for the two felsic intrusions, rules out the presence of large amounts of residual garnet in the source region during melt generation, implying that melting of the subducted slab did not contribute to magma genesis. The Nb depletion shown by all lithologies within the succession is likely related to Nb retention in the dehydrating slab (probably in residual rutile), which could be further enhanced by assimilation of Nb-depleted crustal rocks during magma ascent through the crust.

Generation of the Cosmos volcanic sequence via assimilation of a crustal component and/or crustal anatexis, rather than by partial melting of peridotite contaminated by subducted crustal material, could in theory produce the geochemical characteristics of the volcanic sequence. However, this would require an extremely enriched crustal component, more enriched than estimates of either modern or Archaean continental crust (e.g., Rudnick and Fountain, 1995; Taylor and McLennan, 1985) or of average TTG/D (e.g. Drummond et al., 1996; Smithies, 2000). Contamination by average TTG/D crust would result in strongly fractionated REE concentrations, which is not shown by the extrusive volcanic sequence. The presence of xenocrystic zircons within the dacitic volcanic rocks indicates that assimilation of pre-existing crustal components, which are dated at ~2750 Ma, contributed to the Cosmos volcanic succession (de Joux et al., 2013). However, as only two xenocrystic zircons were found in 52 concordant analyses from numerous felsic volcanic lithologies within the succession, the contribution of assimilated crustal material is likely to have been relatively minor (de Joux et al., 2013). It is not possible to further quantify the contribution of crustal

ACCEPTED MANUSCRIPT

assimilation during magma ascent within the volcanic succession without the use of combined radiogenic isotope ratios such as Pb and Nd. Additionally, no older, suitable potential crustal contaminant, strongly enriched in LREE and LILEs, has been described within the local region. It is therefore considered that the geochemical characteristics of the Cosmos extrusive volcanic succession are the result of melting of a fluid-metasomatised peridotite; a process that is characteristic of modern convergent margins.

The similarities in multi-element plots and REE patterns between the felsic volcanic lithologies are striking (Fig.7a-f). This suggests that they share a similar petrological evolution and/or source region. The intermediate units, while having similar LILE concentrations to the felsic units, show markedly different HFSE patterns lacking the strong Sr, Eu and P negative anomalies seen within the felsic volcanic units. Whether these trace element distinctions can be explained by fractional crystallisation alone or whether different source regions and/or contrasting AFC paths are required to account for the compositional distinction between the intermediate and felsic volcanic units as a whole is discussed in Section 7.6.

The two felsic intrusions have a distinct TTG/D affinity, with a trace element and REE geochemistry consistent with partial melting of a metabasic source at pressures high enough to leave residual garnet ± amphibole, but no plagioclase (Drummond and Defant, 1990). HREEs would be strongly partitioned into garnet, which would be left as a restite mineral in the source region following efficient melt segregation and ascent of the HREE-depleted melt. This requires partial melting of a thickened mafic crust or of a subducting slab (e.g., Drummond and Defant, 1990). The footwall felsic intrusion contains two xenocrystic zircons dated at ~2720 Ma and ~2830 Ma, indicating that some minor crustal assimilation occurred during genesis of the parental melt (de Joux et al., 2013). Assimilation and/or crustal anatexis of an earlier TTG/D-affinity crustal component could have played a part in the genesis of the

ACCEPTED MANUSCRIPT

felsic porphyry intrusions, although a greater abundance of xenocrystic zircons might be expected if this process played a large role in melt generation. Given the strong TTG/D affinity of the felsic intrusions, the melt generation processes and possible tectonic regime during intrusion of the felsic porphyries, emplaced after 2670Ma, was likely to be markedly different than those that generated the felsic and intermediate volcanic sequence emplaced between 2736 and 2724 Ma (de Joux et al., 2013).

7.3 TTG/D affinity in the Eastern Goldfields Superterrane (EGS)

Adakites were recognised by Defant and Drummond (1990) as a unique type of modern arc lava. Although controversial (e.g., Macpherson et al., 2006), present-day adakites are considered by many to be generated via melting of young (<25 m.y.) subducting crust (e.g., Drummond et al., 1996; Martin et al., 2005). Adakites show significant similarities to young (~3.5 - 2.5 Ga) Archaean TTG/D granitoids and therefore they may be regarded as possible modern equivalents (e.g., Martin et al., 2005). However, Moyen and Martin (2012) have recently suggested that Archaean TTG/Ds show a wider compositional range than modern adakites and that Archaean TTG/Ds may be generated by both slab melting and crustal anatexis. TTG intrusions compose much of the EGS. TTD volcanic packages are volumetrically less significant than TTG batholiths but it is the common association of TTD volcanic packages with mineralised komatiites that makes the understanding of TTD formation, emplacement mechanisms and possible tectonic setting important (e.g., Fiorentini et al., 2012). The typical features of modern adakite volcanic rocks, characteristics that also distinguish Archaean TTG/D units, are shown in Table 3. It should be noted that every aspect of the description as shown in Table 3 is an essential part of the definition and that no rock should be called TTG/D if it does have all of the characteristics (Moyen and Martin, 2012).

ACCEPTED MANUSCRIPT

The majority of currently published data on the Kalgoorlie Terrane indicates the terrane was dominated by TTD volcanism. The Agnew-Wiluna (AWB) dacitic volcanic rocks are proposed to have a strong TTD affinity (Fiorentini et al., 2012). Three episodes of TTD-affinity volcanism, spanning ~2710 to ~2665 Ma, are recognised within the Kalgoorlie Terrane (Kositcin et al., 2008). The first episode (2707 – 2692 Ma) comprised felsic volcanism associated with komatiites at Black Swan. The second (2687 – 2676 Ma) and third (2669 – 2665 Ma) episodes comprised felsic volcanism, with associated volcaniclastic and epiclastic sedimentation, in the lower Kalgoorlie Sequence, including the Black Flag Group, and upper Kalgoorlie Sequence respectively.

The rhyolitic and dacitic volcanic rocks at Cosmos are distinct in being significantly older (respectively >2736 Ma and 2730 - 2724 Ma; Table 1) than the majority of felsic rocks within the Kalgoorlie Terrane (Fig. 1). The Cosmos rocks are also geochemically distinct, particularly in comparison to the Black Flag Group, which has a strong TTD geochemical signature (Table 3; Krapež and Hand, 2008; Morris and Witt, 1997). The Black Flag Group is used here for comparison with the Cosmos volcanic sequence because there is comprehensive published geochemical data on the Black Flag succession. The latter group comprises a similar suite of basaltic through to rhyolitic lavas and volcaniclastic rocks, which are largely considered not to be related by fractional crystallisation processes (Morris and Witt, 1997). The Black Flag Group is considered to have formed by partial melting of amphibolite whose likely source is subducted ocean crust (Morris and Witt, 1997). The felsic lavas of the Black Flag Group are depleted in HREEs and less enriched in LREEs relative to the Cosmos felsic volcanic rocks (Table 3). They also show no, or slightly positive, Eu anomalies in contrast to the negative Eu anomalies exhibited by the Cosmos felsic volcanic rocks (Fig. 7). The Cosmos dacite lavas and lapilli tuffs lack most of the geochemical attributes indicating TTG/D affinity in volcanic rocks (e.g., $\geq$ 15 wt. % Al_2O_3, Sr >300ppm, Y <18ppm, depleted

ACCEPTED MANUSCRIPT

HREEs, positive Eu anomalies) whereas both the Cosmos felsic porphyry intrusions have a strong TTG/D affinity and are geochemically similar to the Black Flag dacitic rocks (Table 3; Fig. 7o, p).

The Sr/Y vs. Y discrimination diagram has been used to define modern day adakites and typical island-arc volcanic rocks (Fig. 8). The extrusive Cosmos volcanic lithologies and mafic intrusions fall within the island-arc field whereas the felsic intrusions and the Black Flag Group plot in the adakite field, exhibiting much higher Sr/Y ratios and lower Y concentrations (Fig. 8a). Given the potential mobility of Sr during metamorphism it is also useful to use discrimination diagrams involving elements that are considered to be immobile during metamorphism (Fig. 5d). Martin (1986) presented a way to define TTG-affinity rocks using chondrite-normalised La/Yb and Yb (Fig. 8b). TTG rocks typically have high La/Yb ratios and low HREE contents whereas the products of modern BADR arc volcanism have higher HREE concentrations and lower La/Yb ratios (Fig. 8b). The Cosmos extrusive volcanic lithologies plot entirely within the field of modern BADR volcanic arcs confirming their dominantly volcanic-arc signature whereas the felsic intrusions exhibit a much more typical TTG/D affinity.

7.4 Felsic porphyry intrusions and their relation to regional granite plutons

The TTG/D affinity of the felsic intrusions indicates that the melt generation processes and possible tectonic regime in the Cosmos region had evolved from subduction zone to TTD/G magmatism prior to 2670 Ma. Dating of an in-situ volcanic horizon within the Cosmos Ultramafic Sequence, referred to as the AM5 “reactivation” contact (Fig. 2), indicates komatiite volcanism continued in the region after ~2685 Ma (de Joux et al., 2013). The hangingwall felsic intrusion crosscuts the upper contact of the Cosmos Ultramafic

ACCEPTED MANUSCRIPT

Sequence with the overlying hangingwall sedimentary succession (Fig. 2). Thus, this geodynamic transition likely occurred post 2685 Ma and prior to 2670 Ma. The age of this transition is consistent with that suggested for the extensional D1 phase of deformation within the Norseman-Wiluna belt, which includes the AWB, and was accompanied by a change from volcanic-dominated to plutonic-dominated magmatism between ~2685 and 2675 Ma (Weinberg et al., 2003). The slight difference in composition between the two porphyries, coupled with their contrasting ages, indicates they are the product of two separate episodes of felsic intrusive activity and are likely related to regional granite emplacement.

Champion and Sheraton (1997) divided the granites and granite gneisses of the EGS into five groups: high-Ca, low-Ca, high-HFSE, mafic, and syenitic. The high-Ca and low-Ca groups comprise over 80% of the granite occurrence within the EGS. Figure 9 shows that the Cosmos felsic intrusions are geochemically most similar to the high-Ca granitoids and are thus likely related to the local emplacement of high-Ca granitoid plutons. The felsic porphyry intrusions also show LILE enrichment, appreciable negative Nb anomalies and high Sr, which is typical of high-Ca granites (Fig. 7o). This granite group shares many features with typical Archaean TTG suites. Derivation of high-Ca granites is thought to have occurred at high pressures within a thickened crust or by crustally contaminated slab-derived melts (Champion and Sheraton, 1997). High-Ca granitoids occur immediately west of the AWB and are by far the most abundant granite type in the region, followed by the low-Ca plutons that dominate the central granitoid region between the Agnew-Wiluna and Yandal greenstone belts (Fig. 1). The high-Ca granitoids in this region were emplaced between ~2720 – 2655 Ma whereas low-Ca and syentitic granitoids were emplaced after 2660 Ma (Liu et al., 2002). This change in granite composition has been interpreted to represent a fundamental change in the tectonic environment post ~2660 - 2655Ma, from crustal shortening and voluminous high-Ca granitoids to a tensional environment favouring low-Ca and syentitic magmatism

ACCEPTED MANUSCRIPT

(Smithies and Champion, 1999). The composition and age of the Cosmos felsic porphyry intrusions (Figs. 2, 9) is consistent with regional granite plutonism.

7.5 The intermediate to felsic Cosmos volcanic succession – a high-K calc-alkaline to shoshonite continental arc

The Cosmos extrusive volcanic succession has been shown to have a strong volcanic-arc affinity (Fig. 8). The succession appears to be strongly enriched in LREEs and LILEs compared to the majority of modern and ancient arc successions (Fig. 7) and volcanic lithologies plot within the continental margin region on Figure 10. The less enriched andesites straddle the calc-alkaline-shoshonite boundary, with the more felsic volcanic units plotting distinctly in the shoshonite field (as defined by Manikyamba et al., 2012; Fig. 10). The modern shoshonite rock association is characterised by high Na_2O and K_2O, high LILE content, high but variable Al_2O_3, high Fe_2O_3/FeO and low TiO_2 (e.g., Morrison, 1980). Given that Figure 10 does not define high-K calc-alkaline affinity, and that the volcanic units are grouped relatively close to the shoshonite-calc-alkaline boundary, the Cosmos volcanic sequence is likely to originally have had a high-K calc-alkaline to shoshonite affinity. In modern continental margins, and some island arc settings, there is often a complete gradation between calc-alkaline, high-K calc-alkaline and shoshonitic suites (Morrison, 1980). Therefore, it is not surprising that the Cosmos volcanic sequence straddles the calc-alkaline and shoshonite boundary (Fig. 10).

7.6 Can the intercalated andesite and dacite volcanic units be related by AFC processes?

The intercalated nature of the andesitic units with the dacitic units might imply that they are the less evolved and more evolved products respectively of the same magma source

ACCEPTED MANUSCRIPT

(Fig. 3). However, differing REE patterns, as well as distinct variations on multi-element plots (Fig. 7) indicate the andesitic and dacitic units are unlikely be related by simple fractional crystallisation. Assimilation and fractional crystallisation (AFC) modelling further indicates that the andesite lavas cannot be related to the dacite lavas via AFC processes. A crystallising gabbroic assemblage from the northern Marianas Islands, with an average composition of PLAG:CPX:MAG:OLIV = 60:25:10:5 (Woodhead, 1988), was used for AFC modelling. The AFC equation of De Paolo (1981) was used to assess whether a similar composition to the dacite lavas can be derived, from the least evolved basaltic andesite, when assimilation of crust is included. Modelling also included variable proportions of apatite as a crystallising phase, with a proportional reduction in the other four phases. Within the AWB there is no published data on the possible composition of the local basement to the region's greenstone belt sequences thus several different proto-crust compositions have been modelled. The Archaean felsic average from Rudnick and Fountain (1995) was used as one contaminant. However, even at high r factors (rate of assimilation relative to the rate of crystallisation), enriched compositions such as those of the dacite lavas cannot be produced via AFC processes from the least evolved basaltic andesite lava (Fig. 11b, c). The Archaean felsic average volcanic itself has a lower Th/Yb ratio than the enriched dacite lavas (Fig. 10). Therefore to generate an enriched dacite composition from a basaltic andesite parent melt, the composition of the contaminating crust would have to be substantially more enriched than the Archaean felsic average.

Czarnota et al. (2010) proposed that the Youanmi Terrane may form the basement to the Kalgoorlie Terrane. Consequently a felsic volcanic rock from the Greensleeves formation of the Pollelle Group within the Youanmi Terrane has also been tested as a potential contaminant (Wyman and Kerrich, 2012). This group is dated at ~2760 Ma (Wyman and Kerrich, 2012), which is similar in age to the two xenocrystic zircons dated within the felsic

ACCEPTED MANUSCRIPT

footwall (~2750 - 2760 Ma), making it a feasible crustal contaminant for generation of the Cosmos felsic volcanic sequence. However, AFC processes cannot produce compositions with high enough Th/Yb from the least evolved basaltic andesite, even in the presence of apatite, (Fig. 11d, e). The same is also true when average TTG is used as a crustal contaminant (Fig. 11f; Drummond and Defant, 1996)

The combined effect of fractional crystallisation in the presence of apatite with contamination by either the Archaean felsic average or a felsic volcanic from the Pollelle group increases the Th/Yb and Nb/Yb ratios, but requires both high r factors and fractional crystallisation including ≥2% apatite. This still does not reproduce the high Th/Yb ratios in the dacite lavas, although contamination by a more enriched source lithology cannot be ruled out. Nevertheless, given the large proportion of assimilation required, and the requirement for ≥2% apatite as a crystallising phase, we conclude that the dacite lavas cannot be related to the andesites via AFC processes. The dacites are considered to be derived from a compositionally distinct source region with a more enriched slab component and/or their parental magmas were produced by lower degrees of partial melting than the andesites. Hastie et al. (2009) utilised differing trace element ratios and isotopic compositions to suggest that the tholeiitic and overlying calc-alkaline island arc lavas from the Cretaceous Devils Racecourse Formation in Jamaica were derived from chemically similar mantle wedge, largely N-MORB, source regions but that these source regions were enriched by chemically distinct slab fluxes. Calc-alkaline rocks were derived from a more enriched mantle source region contaminated with either (a) a more enriched slab component and/or (b) a larger volume of the enriched slab component that that which contaminated the tholeiitic source. Thus, the intercalated andesite and dacite lavas at Cosmos may have had a similar petrogenesis, forming from at least two separate, but coeval, volcanic centres that tapped compositionally different mantle sources.

ACCEPTED MANUSCRIPT

Shoshonite magmatism in the Izu-Bonin-Mariana arc is considered to be derived from melt produced by slab fluxing that affected the composition of the mantle without erupting to the surface (Ishizuka et al., 2010). Melt extraction of part of this metasomatised mantle produced arc volcanism, with subsequent production of shoshonite magma from the same mantle source due to decompression melting upon initiation of rifting. A similar type of process could account for the compositional diversity of the andesites and dacites at Cosmos, given that disruption of the arc by a rising mantle plume may have facilitated back-arc extension and rifting in the EGS subduction zone (Czarnota et al., 2010).

8. Tectonic setting of the Cosmos volcanic succession

8.1 Archaean shoshonites – comparison and importance

Shoshonitic volcanic rocks are found in both modern and ancient terranes. As modern shoshonitic and calc-alkaline volcanism occurs largely in convergent margins with active subduction of oceanic crust or a past history of subduction (Morrison, 1980) modern-style subduction processes have been inferred in the genesis of the equivalent Archaean rock suites (e.g., Dostal and Mueller, 1992; Giles and Hallberg, 1982; Hollings and Kerrich, 2006; Manikyamba et al., 2012). Late Archaean shoshonites are described in the North America's Superior Province including the Timiskaming Group in Ontario (e.g., Corfu et al.,1991)), the Oxford Lake Group (Brooks et al., 1982), the Opemisca Group in Quebec (Dostal and Mueller, 1992), and the 2.7 - 2.8 Ga greenstone terranes of the Uchi greenstone-granite subprovince in Ontario (Hollings and Kerrich, 2006). Late Archaean shoshonites have also been recognised in the western Dharwar Craton of India (Manikyamba et al., 2012). It has been argued that the Superior Province shoshonites represent late-stage magmatic products in volcanic arc settings and, based on geochemical analogy to modern shoshonites, they were

ACCEPTED MANUSCRIPT

derived from mantle sources rich in subduction-related fluids (e.g., Brookes et al., 1982; Dostal and Mueller, 1992; Hollings and Kerrich, 2006). No extrusive shoshonites are recognised within the Yilgarn Craton, with strongly enriched rocks only represented by shoshonitic lamprophyre dykes in the EGS (Taylor et al., 1994). Shoshonitic magmatism manifested as sub-volcanic lamprophyres is spatiotemporally associated with mesothermal gold mineralisation whose emplacement is confined to ~2.6 Ga (Taylor et al., 1994). Calc-alkaline volcanism is recognised within the Kurnalpi and Gindalbie Terranes of the EGS, dated respectively at ~2715 - 2704 Ma and ~2692 - 2680 Ma (e.g., Barley et al., 2008; Giles and Hallberg, 1982). However, TTD volcanic products are much more voluminous throughout the EGS. Thus, although calc-alkaline volcanism has been described in the EGS, the Cosmos volcanic succession is the first recorded strongly enriched high-K calc-alkaline to shoshonite volcanic-arc sequence within the Kalgoorlie Terrane and is unique in being significantly older and more enriched than other arc successions within adjacent terranes of the EGS.

8.2 Island-arc and TTD-affinity volcanism within the Kalgoorlie Terrane

The relative rarity of typical arc-derived volcanic successions within the Kalgoorlie Terrane could be a function of hotter subduction zones within the Archaean (e.g., Kerrich and Polat, 2006). If the Neoarchaean oceanic lithosphere was generally young, this would result in slow, shallow subduction, and, coupled with higher geothermal gradients in the Archaean mantle (e.g., Martin, 1986), would result in hot subduction zones. Moyen and Stevens (2006) considered high pressure TTG/Ds to be the product of fluid-absent melting of metabasite under P/T conditions only likely to be achieved in significantly hotter subduction zones than

ACCEPTED MANUSCRIPT

modern counterparts. Thus, in hot late Archaean subduction zones, partial melting of the subducted oceanic crust, generating typical TTG/D melts, may have been a dominant melt-forming process. However, calc-alkaline BADR volcanic sequences resembling Phanerozoic counterparts, considered to represent extensive intra-oceanic arc systems, exist within the early-late Archaean (e.g., Kerrich and Polat, 2006; Wyman and Kerrich 2009; 2010).

This paper demonstrates that the Cosmos extrusive volcanic footwall succession has geochemical characteristics much more typical of partial melting of peridotite, which had been enriched in the mantle wedge by slab-derived fluids and/or sediment melt. Fiorentini et al. (2012) proposed that TTD-affinity volcanic successions within the AWB formed via partial melting of the mafic lower crust, with ascending komatiitic mantle plumes possibly providing the heat source in a rift or back-arc rift environment. If a back-arc was the tectonic setting of the AWB, an outside heat source, such as a rising mantle plume, would not be required because melting of the down-going slab could occur regardless in a hotter subduction zone. Mantle plume impingement on an active subduction zone could also sufficiently increase the geothermal gradient of the mantle to result in a switch from partial melting of the mantle wedge to melting of the slab itself. Thus, the Cosmos volcanic succession, and TTD-affinity volcanic successions of the Kalgoorlie Terrane, could be formed in the same evolving arc setting.

The incompatible trace element concentrations of individual volcanic units within the Cosmos succession suggest derivation from at least two distinct mantle sources that were influenced by either one or a combination of the following: different mantle sources, differing degrees of partial melting or sources that experienced contrasting sediment and/or slab-derived fluid input from the subducting slab. A later switch to more partial melts derived via melting of the subducting oceanic crust could have formed the typical TTG/D-melts seen regionally within the Kalgoorlie Terrane. More detailed geochemical examination of the TTD

ACCEPTED MANUSCRIPT

affinity of felsic volcanic sequences within the Agnew-Wiluna Belt and the wider Kalgoorlie Terrane needs to be undertaken to determine what proportion of TTD volcanism shows characteristics of the high pressure TTD sub-group that can only be attributed to derivation via slab melting in a subduction setting (Moyen and Martin, 2012). The ~15 – 20 Ma age difference between the Cosmos volcanic arc succession and the neighbouring Mount Keith and Perseverance successions leaves ample time for the evolution of an arc system and a transition from mantle derived partial-melts above the subducting slab, to partial melting of the down-going slab itself. Defant and Kepezkinkas (2001) show that the transition from arc basalts to adakites in modern arcs settings may occur in only a few million years.

Defant and Drummond (1990) recognise that both partial melting of the oceanic crust and flux melting of the mantle wedge can contribute "simultaneously" to active volcanism in a subduction zone, forming the arc volcanoes of Mount St Helens and Mount Adams respectively. Similar processes may have operated within Archaean arcs. Czarnota et al. (2010) linked the Kalgoorlie, Kurnalpi and Burtville Terranes within a westward-dipping subduction zone active between ~2715 and 2690 Ma. The Kalgoorlie Terrane is considered to represent a back-arc setting where minor calc-alkaline volcanism within the Kalgoorlie sequence, generated by partial melting of the mantle wedge is suggested to have occurred contemporaneously with slab-melting producing the high-Ca granite magmatism between 2690 and 2670 Ma (Czarnota et al., 2010). Given that the Cosmos succession is ~10 - 20 Ma older than the volcanic sequences within the Kalgoorlie Terrane, it either represents an earlier phase of arc volcanism within the EGS arc-system or may be a separate arc-fragment that became accreted onto the Kalgoorlie Terrane prior to voluminous high-Ca granite intrusion between 2690 and 2670 Ma (Czarnota et al., 2010).

ACCEPTED MANUSCRIPT

8.3 Mantle plume – volcanic arc interaction in the EGS

At present, the current dating constraints on the emplacement of the lower part of the Cosmos Ultramafic Sequence, UMu1, are bracketed by the ~2724 Ma age of the underlying and ~2685 Ma age of the overlying felsic volcanic sequences along the AM5 "reactivation" contact (Fig. 2; de Joux et al., 2013). Emplacement of the UMu1 package could have occurred at any point within this timeframe. de Joux et al. (2013) discussed the possibility that the contact between the UMu1 package and its underlying footwall volcanic sequence described here may represent a significant unconformity, representing a major hiatus in volcanism in the region. Ultramafic volcanism at Cosmos could be coeval with ultramafic volcanism in the eastern segment of the AWB, where Re/Os and U-Pb dating indicates emplacement ages between ~ 2713 - 2700 Ma for the Mount Keith and Perseverance felsic and ultramafic sequences (Rosengren et al., 2008; Fiorentini et al., 2012). Given the regional nature of ultramafic volcanism within the Kalgoorlie Terrane it is suggested that the emplacement of the Cosmos UMu1 package is related to the main Kalgoorlie komatiite event (Campbell and Hill, 1988; Barnes et al., 2012). Consequently, the most likely emplacement age is at ca. 2707 Ma, although emplacement up to ~20 Ma before or after this date cannot be ruled out.

Komatiite volcanism throughout the AWB, and wider Kalgoorlie Terrane, is considered to result from either a plume within a back-arc region of a subduction zone (e.g., Czarnota et al., 2010), or a larger plume head that was deflected from beneath the Youanmi Terrane to the west (Barnes et al., 2012). The volcanic arc affinity of the Cosmos footwall sequence provides strong evidence that plume-only geodynamic scenarios cannot account for the compositional diversity of volcanic sequences in the AWB.

Coeval eruption of plume and arc-related volcanic sequences are described from the southern Abitibi belt, where the existence of arc-type rocks prior to plume ascent and the very

ACCEPTED MANUSCRIPT

close association of a mantle plume with renewed subduction is taken to indicate direct interaction between these two geodynamic regimes (Wyman and Kerrich, 2009; 2010). In the northern volcanic zone of the Abitibi belt Dostal and Mueller (1997) considered the conformable association of calc-alkaline felsic volcanic rocks of the Hunter Mine group with the overlying basalts and komatiites of the Stoughton-Roquemaure Group to represent the rise of a mantle plume beneath and through a volcanic arc complex. Furthermore the latter authors consider that rifting was initiated and enhanced by the rising plume.

A similar situation is considered for the AWB, and wider EGS, where the Cosmos volcanic sequence records the earliest record of subduction between ~2736 – 2724 Ma. The active arc was then subsequently disrupted by the impingement of an ascending mantle plume resulting in widespread komatiitic volcanism at ca. 2707 Ma (Kositcin et al., 2008). The presence of a plume in the back arc region of the EGS subduction zone, as suggested by Czarnota et al. (2010), would have raised the geothermal gradient of the subduction zone and promoted slab melting, rather than partial melting in the mantle wedge, facilitating a transition to TTD/G volcanism in the east of the AWB and later the wider EGS.

9. Conclusions

The Cosmos volcanic succession represents the first extrusive, high-K calc-alkaline to shoshonitic volcanic arc sequence described in the Kalgoorlie Terrane, if not the whole of the EGS. The only units present within the Cosmos succession to show a TTG/D affinity are the significantly younger felsic porphyry intrusions that are linked to local high-Ca granitoid intrusive activity. Thus, the Agnew-Wiluna belt is not wholly composed of intermediate and felsic volcanic sequences with a TTD-affinity as suggested by Fiorentini et al. (2012). Given

ACCEPTED MANUSCRIPT

that the Cosmos volcanic succession is ~15 - 25 Ma older than the majority of felsic rocks within the AWB (de Joux et al., 2013) and has a different and distinct geochemical affinity, it may represent a separate arc terrane in its own right that experienced subsequent accretion with the Kalgoorlie Terrane. Alternatively the geochemical affinity and thus potential tectonic setting of the Agnew-Wiluna greenstone belt itself may be more complex than currently considered suggesting that surrounding felsic successions require further detailed geochemical assessment to establish if they do in fact all exhibit a true TTG/D affinity. Unravelling the apparent tectonic complexity of the region is particularly important given the recent re-ignition of the plume-dominated versus subduction accretion debate for the origin for the EGS (Barnes et al., 2012). Recognition of this distinct high-K calc-alkaline to shoshonite island-arc sequence associated with komatiites suggests that mantle plume – volcanic arc interaction occurred in the EGS. The Cosmos succession also provides further evidence that modern style plate tectonics were operating during the late Archaean, contrary to the assertion of Bédard et al. (2013) that evidence for Archaean island arcs is sparse because they did not exist.

10. Acknowledgements

The authors would like to thank Xstrata Nickel Australasia for funding this research; in particular the authors would like to thank Steve Vallance and Peter Langworthy who initiated this research project under Jubilee Mines, and Don Huntly, Graham Leaver and Terry Mallinson for their continued support of the research under Xstrata Nickel Australasia. We also want to thank all past Cosmos Exploration staff for their support during data collection in the field. We thank Nic Odling at the University of Edinburgh and Valerie Olive at SUERC who provided valuable assistance and guidance during sample preparation and

ACCEPTED MANUSCRIPT

analysis via XRF and ICP-MS respectively. Special thanks are extended to Michael Denny for constructive and thorough comments on early drafts of this paper.

11. References

Barley, M.E., Brown, S.J., Krapež, B., Kositcin, N., 2008. Physical volcanology and geochemistry of a Late Archaean volcanic arc: Kurnalpi and Gindalbie Terranes, Eastern Goldfields Superterrane, Western Australia. Precambrian Research 161 (1), 53-76.

Barnes, S.J., Hill, R.E.T., Gole, M.J., 1988. The Perseverance ultramafic complex, Western Australia: the product of a komatiite lava river. Journal of Petrology 29 (2), 305-331.

Barnes, S.J., Van Kranendonk, M.J., Sonntag, I., 2012. Geochemistry and tectonic setting of basalts from the Eastern Goldfields Superterrane, Australian Journal of Earth Science: An International Geoscience journal of the Geological Society of Australia 59 (5), 707-735.

Bau, M., 1991. Rare-earth element mobility during hydrothermal and metamorphic fluid-rock interaction and the significance of the oxidation state of europium. Chemical Geology 93 (3), 219-230.

Bédard, J.H, Harris, L.B., Thurston, P.C. 2013. The hunting of the snArc. Precambrian Research 229, 20-48.

Boynton, N.L., 1984. Geochemistry of the rare earth elements: meteorite studies. In: Henderson, P. (Eds.), Rare Earth Element Geochemistry, Elsevier, pp. 63 - 114.

ACCEPTED MANUSCRIPT

Brooks, C., Ludden, J., Pigeon, Y., Hubregtse, J.J.M.W., 1982. Volcanism of shoshonite to high-K andesite affinity in an Archaean arc environment, Oxford Lake, Manitoba. Canadian Journal of Earth Sciences 19 (1), 55-67.

Campbell, I.H., Hill, R.I., 1988. A two-stage model for the formation of the granite-greenstone terrains of the Kalgoorlie-Norseman area, Western Australia. Earth and Planetary Science Letters 90 (1), 11-25.

Cassidy, K.F., Champion, D.C., Krapež, B., Barley, M.E., Brown, S.J.A., Blewett, R.S., Groenewald P.B., Tyler, I.M., 2006. A revised geological framework for the Yilgarn Craton, Western Australia. Western Australia Geological Survey, Record 2006/8, 8 pp.

Champion, D.C., Sheraton, J.W., 1997. Geochemistry and Nd isotope systematics of Archaean granites of the Eastern Goldfields, Yilgarn Craton, Australia: implications for crustal growth processes. Precambrian Research 83 (1), 109-132.

Corfu, F., Jackson, S.L., Sutcliffe, R.H. 1991. U-Pb ages and tectonic significance of late Archean alkalic magmatism and nonmarine sedimentation: Timiskaming Group, southern Abitibi belt, Ontario. Canadian Journal of Earth Sciences, 28(4), 489-503.

Czarnota, K., Champion, D.C., Goscombe, B., Blewett, R.S., Cassidy, K.F., Henson, P. A., Groenewald, P.B., 2010. Geodynamics of the eastern Yilgarn Craton. Precambrian Research 183 (2), 175-202.

Defant, M.J., Drummond, M.S., 1990. Derivation of some modern arc magmas by melting of young subducted lithosphere. Nature 347 (6294), 662-665.

Defant, M.J., Kepezhinskas, P., 2001. Evidence suggests slab melting in arc magmas. Eos, Transactions American Geophysical Union 82 (6), 65-69.

ACCEPTED MANUSCRIPT

de Joux, A., Thordarson, T., Denny, M., Hinton, R.W., de Joux A.J., 2013. U-Pb dating constraints on the felsic and intermediate volcanic sequence of the nickel-sulphide bearing Cosmos succession, Agnew-Wiluna greenstone belt, Yilgarn Craton, Western Australia. Precambrian Research 236, 86-105.

De Paolo, D. J., 1981. Trace element and isotopic effects of combined wallrock assimilation and fractional crystallization. Earth and Planetary Science Letters 53 (2), 189-202.

Dostal, J., Mueller, W., 1992. Archaean shoshonites from the Abitibi greenstone belt, Chibougamau (Québec, Canada): geochemistry and tectonic setting. Journal of Volcanology and Geothermal Research 53 (1), 145-165.

Dostal, J., Mueller, W.U., 1997. Komatiite Flooding of a Rifted Archean Rhyolitic Arc Complex: Geochemical Signature and Tectonic Significance of the Stoughton-Roquemaure Group, Abitibi Greenstone Belt, Canada. The Journal of Geology 105, 545-564.

Drummond, M.S., Defant, M.J., 1990. A model for trondhjemite–tonalite–dacite genesis and crustal growth via slab melting: Archaean to modern comparisons. Journal of Geophysical Research 95, 21503–21521.

Drummond, M.S., Defant, M.J., Kepezhinskas P.K., 1996. Petrogenesis of slab-derived trondhjemite-tonalite-dacite/adakite magmas. Transactions of the Royal Society of Edinburgh-Earth Sciences 87 (1), 205-216.

Fiorentini, M., Beresford, S., Barley, M., Duuring, P., Bekker, A., Rosengren, N., Cas, R., Hronsky, J., 2012. District to camp controls on the genesis of komatiite-hosted nickel

ACCEPTED MANUSCRIPT

sulfide deposits, Agnew-Wiluna greenstone belt, Western Australia: Insights from the multiple sulfur isotopes. Economic Geology 107(5), 781-796.

Floyd, P.A., Winchester, J.A., 1978. Identification and discrimination of altered and metamorphosed volcanic rocks using immobile elements. Chemical Geology 21(3), 291-306.

Gee, M., Swager, C., 2008. Late Archaean volcanic arcs and their accretionary history, Eastern Goldfields Superterrane: Plate tectonic models inferred from tectonostratigraphic analysis. Precambrian Research 161 (1), 1-4.

Giles, C.W., Hallberg, J.A., 1982. The genesis of the Archaean Welcome Well volcanic complex, Western Australia. Contributions to Mineralogy and Petrology 80 (4), 307-318.

Hamilton, W.B., 2003. An alternative earth. GSA Today 13 (11), 4-12.

Hastie, A. R., Kerr, A. C., Mitchell, S. F., Millar, I. L. 2009. Geochemistry and tectonomagmatic significance of Lower Cretaceous island arc lavas from the Devils Racecourse Formation, eastern Jamaica. Geological Society, London, Special Publications, 328(1), 339-360.

Hill, R.E.T. Barnes, S.J. Gole, M.J. Dowling, S.E., 1995. The volcanology of komatiites as deduced from field relationships in the Norseman-Wiluna greenstone belt, Western Australia. Lithos 34 (1-3), 159-188.

Hill, R.E.T., Barnes, S.J., Dowling, S.E., Thordarson, T., 2004. Komatiites and nickel sulphide ore bodies of the Black Swan area, Yilgarn Craton, Western Australia. 1. Petrology and volcanology of host rocks. Mineralium Deposita 39(7), 684-706.

ACCEPTED MANUSCRIPT

Hill, R.E.T., Dowling, S.E., 2008. The petrology and geochemistry of mineralised komatiites intersected in three diamond drill holes (AM262B, AMD275 and BJD048A) from the AM5 Nickel Sulphide Deposit; Cosmos region, Agnew-Wiluna Greenstone Belt; A pilot study for characterising mineralised domains within the ore body. Unpublished External report, Kalapana Research Associates and Triodia Research.

Hollings, P., Kerrich, R., 2006. Light rare earth element depleted to enriched basaltic flows from 2.8 to 2.7 Ga greenstone belts of the Uchi Subprovince, Ontario, Canada. Chemical Geology 227(3), 133-153.

Ishizuka, O., Yuasa, M., Tamura, Y., Shukuno, H., Stern, R.J., Naka, J., Joshima, M., Taylor, R.N., 2010. Migrating shoshonitic magmatism tracks Izu-Bonin-Mariana intra-oceanic arc rift propagation. Earth and Planetary Science Letters 294, 111-122.

Johnson, M.C., Plank, T., 1999. Dehydration and melting experiments constrain the fate of subducted sediments. Geochemistry Geophysics Geosystems, 1 GC000014.

Kerrich, R., Polat, A., 2006. Archean greenstone-tonalite duality: Thermochemical mantle convection models or plate tectonics in the early Earth global dynamics? Tectonophysics 415 (1), 141-165.

Kositcin, N., Brown, S.J., Barley, M.E., Krapež, B., Cassidy, K.F., Champion, D.C., 2008. SHRIMP U-Pb zircon age constraints on the Late Archaean tectonostratigraphic architecture of the Eastern Goldfields Superterrane, Yilgarn Craton, Western Australia. Precambrian Research 161 (1), 5-33.

Krapež, B., Hand, J.L. 2008. Late Archaean deep-marine volcaniclastic sedimentation in an arc-related basin: the Kalgoorlie Sequence of the Eastern Goldfields Superterrane, Yilgarn Craton, Western Australia. Precambrian Research 161 (1), 89-113.

ACCEPTED MANUSCRIPT

Le Bas, M.J., Le Maitre, R.W., Streckeisen, A., Zanettin, B., 1986. A chemical classification of volcanic rocks based on the total alkali-silica diagram. Journal of Petrology 27 (3), 745-750.

Lemarchand, F., Villemant, B., Calas, G. 1987. Trace element distribution coefficients in alkaline series. Geochimica et Cosmochimica Acta 51 (5), 1071-1081.

Ludden, J., Gélinas, L., Trudel, P., 1982. Archaean metavolcanics from the Rouyn-Noranda district, Abitibi Greenstone Belt, Quebec. 2. Mobility of trace elements and petrogenetic constraints. Canadian Journal of Earth Sciences 19 (12), 2276-2287.

Liu, S.F., Champion, D.C., Cassidy K.F., 2002. Geology of the Sir Samuel 1:250,000 sheet area, Western Australia Geoscience Australia Record 14.

Mahood, G.A., Stimac, J.A. 1990. Trace-element partitioning in pantellerites and trachytes. Geochimica et Cosmochimica Acta 54 (8), 2257-2276.

Manikyamba, C., Kerrich, R., Polat, A., Raju, K., Satyanarayanan, M., Krishna, A.K., 2012. Arc Picrite-Potassic Adakitic-Shoshonitic Volcanic Association of the NeoArchaean Sigegudda Greenstone Terrane, Western Dharwar Craton: Transition from Arc Wedge to Lithosphere Melting. Precambrian Research 212, 207-224.

Martin, H., 1986. Effect of steeper Archaean geothermal gradient on geochemistry of subduction-zone magmas. Geology 14, 753–756.

Martin, H., 1994. The Archaean grey gneisses and the genesis of continental crust. In: Condie, K. C. (Eds.) Archaean Crustal Evolution. Amsterdam: Elsevier, pp.205–259.

Martin, H., 1999. Adakitic magmas: modern analogues of Archaean granitoids. Lithos 46, 411-429.

ACCEPTED MANUSCRIPT

Martin, H., Smithies, R.H., Rapp, R., Moyen, J.F., Champion, D. 2005. An overview of adakite, tonalite–trondhjemite–granodiorite (TTG), and sanukitoid: relationships and some implications for crustal evolution. Lithos 79(1), 1-24.

Masuda, A., Nakamura, N., Tanaka, T., 1973. Fine structures of mutually normalized rare-earth patterns of chondrites. Geochimica et Cosmochimica Acta 37(2), 239-248.

McKenzie, D.A.N., O'nions, R.K. 1991. Partial melt distributions from inversion of rare earth element concentrations. Journal of Petrology 32 (5), 1021-1091.

Macpherson, C.G., Dreher, S.T., Thirlwall, M.F. 2006. Adakites without slab melting: high pressure differentiation of island arc magma, Mindanao, the Philippines. Earth and Planetary Science Letters 243(3), 581-593.

Michard, A., Albarède, F., 1986. The REE content of some hydrothermal fluids. Chemical Geology 55 (1), 51-60.

Morris, P.A., Witt, W.K., 1997. Geochemistry and tectonic setting of two contrasting Archaean felsic volcanic associations in the Eastern Goldfields, Western Australia. Precambrian Research 83(1), 83-107.

Morrison, W., 1980. Characteristics and tectonic setting of the shoshonite rock association. Lithos 13 (1), 97-108.

Moyen, J.F., Martin, H., 2012. Forty years of TTG research. Lithos 48, 312-336.

Moyen, J.F., Stevens, G., 2006. Experimental constraints on TTG petrogenesis: implications for Archaean geodynamics. Benn, K., Mareschal, J., Condie, K.C., (Eds.), Archaean geodynamics and environments, American Geophysical Union, Washington, pp. 149-175.

ACCEPTED MANUSCRIPT

Nelson, D.R., 1997. Evolution of the Archaean granite-greenstone terranes of the Eastern Goldfields, Western Australia: SHRIMP U-Pb zircon constraints. Precambrian Research 83 (1), 57-81.

Nelson, D.R., 1998. Granite–greenstone crust formation on the Archaean Earth: a consequence of two superimposed processes. Earth and Planetary Science Letters 158(3), 109-119.

Pawley, M.J., Wingate, M.T.D., Kirkland, C.L., Wyche, S., Hall, C.E., Romano, S.S., Doublier, M.P., 2012. Adding pieces to the puzzle: episodic crustal growth and a new terrane in the northeast Yilgarn Craton, Western Australia. Australian Journal of Earth Sciences 59 (5), 603-623.

Pearce, J.A., 2008. Geochemical fingerprinting of oceanic basalts with applications to ophiolite classification and the search for Archaean oceanic crust. Lithos 100(1), 14-48.

Pearce, J.A., Peate, D.W., 1995. Tectonic implications of the composition of volcanic arc magmas. Annual Reviews in Earth Planetary Science 23, 251–285.

Pearce, J.A., Norry, M.J. 1979. Petrogenetic implications of Ti, Zr, Y, and Nb variations in volcanic rocks. Contributions to Mineralogy and Petrology 69 (1), 33-47.

Peccerillo, A., Taylor, S.R., 1976. Geochemistry of Eocene calc-alkaline volcanic rocks from the Kastamonu area, northern Turkey. Contributions to Mineralogy and Petrology 58 (1), 63-81.

Rickwood, P.C., 1989. Boundary lines within petrologic diagrams which use oxides of major and minor elements. Lithos 22 (4), 247-263.

ACCEPTED MANUSCRIPT

Rosengren, N.M., Cas, R.A.F., Beresford, S.W., Palich, B.M., 2008. Reconstruction of an extensive Archaean dacitic submarine volcanic complex associated with the komatiite-hosted Mt Keith nickel deposit, Agnew-Wiluna greenstone belt, Yilgarn Craton, Western Australia. Precambrian Research 161 (1), 34-52.

Rudnick, R.L., Fountain, D.M., 1995. Nature and composition of the continental crust: a lower crustal perspective. Reviews of Geophysics 33 (3), 267-309.

Schock, H.H. 1979. Distribution of rare-earth and other trace elements in magnetites. Chemical Geology 26 (1), 119-133.

Smithies, R.H., 2000. The Archaean tonalite–trondhjemite–granodiorite (TTG) series is not an analogue of Cenozoic adakite. Earth and Planetary Science Letters 182 (1), 115-125.

Smithies, R.H., Champion, D.C. 1999. Late Archaean felsic alkaline igneous rocks in the Eastern Goldfields, Yilgarn Craton, Western Australia: a result of lower crustal delamination? Journal of the Geological Society 156 (3), 561-576.

Sun, S.S., McDonough, W., 1989. Chemical and isotopic systematics of oceanic basalts: implications for mantle composition and processes. Geological Society, London, Special Publications 42 (1), 313-345.

Taylor, S.R., McLennan, S.M., 1985. The continental crust: its composition and evolution. Reviews of Geophysics 33 (2), 241-265.

Taylor, W.R., Rock, N., Groves, D.I., Perring, C.S., Golding, S.D., 1994. Geochemistry of Archaean shoshonitic lamprophyres from the Yilgarn Block, Western Australia: Au abundance and association with gold mineralization. Applied Geochemistry 9 (2), 197-222.

ACCEPTED MANUSCRIPT

Trofimovs, J., Tait, M.A., Cas, R.A.F., McArthur, A., Beresford, S.W. 2003. Can the role of thermal erosion in strongly deformed komatiite–Ni–Cu–(PGE) deposits be determined? Perseverance, Agnew–Wiluna Belt, Western Australia. Australian Journal of Earth Sciences 50 (2), 199-214.

Trofimovs, J., Davis, B.K., Cas, R.A.F., 2004. Contemporaneous ultramafic and felsic intrusive and extrusive magmatism in the Archaean Boorara Domain, Eastern Goldfields Superterrane, Western Australia, and its implications. Precambrian Research 131 (3), 283-304.

Weinberg, R.F., Moresi, L., van der Borgh, P., 2003. Timing of deformation in the Norseman-Wiluna belt, Yilgarn Craton, Western Australia. Precambrian Research 120 (3), 219-239.

Whitford, D.J., Korsch, M.J., Porritt, P.M., Craven, S. J., 1988. Rare-earth element mobility around the volcanogenic polymetallic massive sulfide deposit at Que River, Tasmania, Australia. Chemical Geology 68 (1), 105-119.

Winchester, J.A., Floyd, P.A., 1977. Geochemical discrimination of different magma series and their differentiation products using immobile elements. Chemical Geology 20, 325-343.

Woodhead, J.D., 1988. The origin of geochemical variations in Mariana lavas: a general model for petrogenesis in intra-oceanic island arcs? Journal of Petrology 29(4), 805-830.

Wyman, D.A., 2013. A critical assessment of Neoarchean “plume only” geodynamics: Evidence from the Superior Province. Precambrian Research 229, 3-19.

ACCEPTED MANUSCRIPT

Wyman, D., Kerrich, R., 2010. Mantle plume - volcanic arc interaction: Consequences for magmatism, metallogeny, and cratonization in the Abitibi and Wawa subprovinces, Canada. Canadian Journal of Earth Sciences 47, 565-589.

Wyman, D., Kerrich, R., 2009. Plume and arc magmatism in the Abitibi subprovince: Implications for the origin of Archean continental lithospheric mantle. Precambrian Research 168, 4-22.

Wyman, D.A., Kerrich, R., 2012. Geochemical and isotopic characteristics of Youanmi terrane volcanism: the role of mantle plumes and subduction tectonics in the western Yilgarn Craton. Australian Journal of Earth Sciences 59 (5), 671-694.

Figure captions

Figure 1. Location maps of the Cosmos mine site within the AWB and its position within the EGS of the Yilgarn Craton, highlighting terrane boundaries and the approximate ages of the different terranes (modified after Cassidy et al., 2006 and de Joux et al., 2013). U-Pb ages from Kositcin et al., (2008) and Pawley et al., (2012).

Figure 2. Generalised vertical section of the Cosmos greenstone stratigraphy including representative core photos and U-Pb ages (modified after de Joux et al., 2013).

ACCEPTED MANUSCRIPT

Figure 3. A -200m (below sea level) level plan through the succession, which, given the subvertical dip of the succession, may represent a north-south cross-section through the primary volcanic stratigraphy.

Figure 4. (a-f). Variation plots against TiO_2 of major elements for different lithological units within the stratigraphy. Individual analyses have been recalculated to 100% on a volatile-free basis.

Figure 5. (a-f) Incompatible element plots against Zr to highlight trace element immobility; concentrations in ppm.

Figure 6. Compositional diagrams (after Winchester and Floyd, 1977) showing the composition of the main lithological groups.

Figure 7. REE and multi-element plots for each of the six main extrusive footwall lithologies as well as the mafic and felsic intrusions. REE plots are normalised to the chondrite values of Boynton (1984). Multi-element plots are normalised to the N-MORB values of Sun and McDonough (1989). The compositional field of the Black Flag rhyolites (dark grey), dacite (medium grey) and andesite (light grey) are shown for reference (data from Morris and Witt, 1997).

ACCEPTED MANUSCRIPT

Figure 8. (A) Sr/Y vs. Y diagram (after Defant and Drummond (1990) and Drummond and Defant (1990)) modified after de Joux et al. (2013). (B) $(La/Yb)_N$ vs. Yb_N after Martin (1986). La/Yb_N is chondrite normalised using the values from Masuda et al. (1973) divided by 1.2, after Moyen and Martin (2012). Black Flag Group data from Morris and Witt (1997).

Figure 9. Yilgarn granite discrimination diagrams (after Champion and Sheraton, 1997) showing the geochemical composition of the footwall and hangingwall felsic porphyry intrusions. Sr/Sr* is primordial mantle-normalised Sr abundance divided by the interpolated value obtained by averaging the normalised Ce and Nd concentrations (Primordial mantle normalising values from Sun and McDonough, 1989).

Figure 10. Th/Yb vs. Nb/Yb discrimination diagram after Pearce (2008) and Manikyamba et al. (2012). Shoshonite (SHO), calc-alkaline (CA) and tholeiite (TH) are shown after Manikyamba et al. (2012). S, subduction component vector; C, crustal contamination vector; W, within plate variation; f, fractional crystallization (after Manikyamba et al. 2012). Primordial mantle, Archaean mantle and Archaean felsic average are taken from Pearce (2008) and references therein. FW = Footwall, HW = Hangingwall, Gt-Hb = garnet-hornblende.

Figure 11. AFC modelling of the least evolved basaltic andesite to test the hypothesis that a composition close to that of the dacite lavas can be achieved by AFC processes. Fractional crystallisation modelling was carried out using a crystallising gabbroic assemblage with the average composition of PLAG:CPX:MAG:OLIV = 60:25:10:5 (after Woodhead, 1988). Modelling including apatite as a crystallising phase was also used (10. B, C, E). **(A-C)** AFC

ACCEPTED MANUSCRIPT

modelling (De Paolo, 1981) using Archaean felsic average (Rudnick and Fountain, 1995), **(D, E)** AFC modelling using, CUE-21, an evolved felsic volcanic rock from the Youanmi Terrane (Wyman and Kerrick, 2012). **(F)** AFC modelling using Average TTG (Rudnick and Fountain, 1995). Distribution coefficients for crystallising phases were obtained from McKenzie and O'Nions (1991; plagioclase, clinopyroxene and olivine), Mahood and Stimac (1983; apatite – Th, Yb), Pearce and Norry (1979; apatite - Nb), Lemarchand et al. (1987; magnetite – Th, Yb) and Schock (1979; magnetite - Nb).

ACCEPTED MANUSCRIPT

ACCEPTED MANUSCRIPT

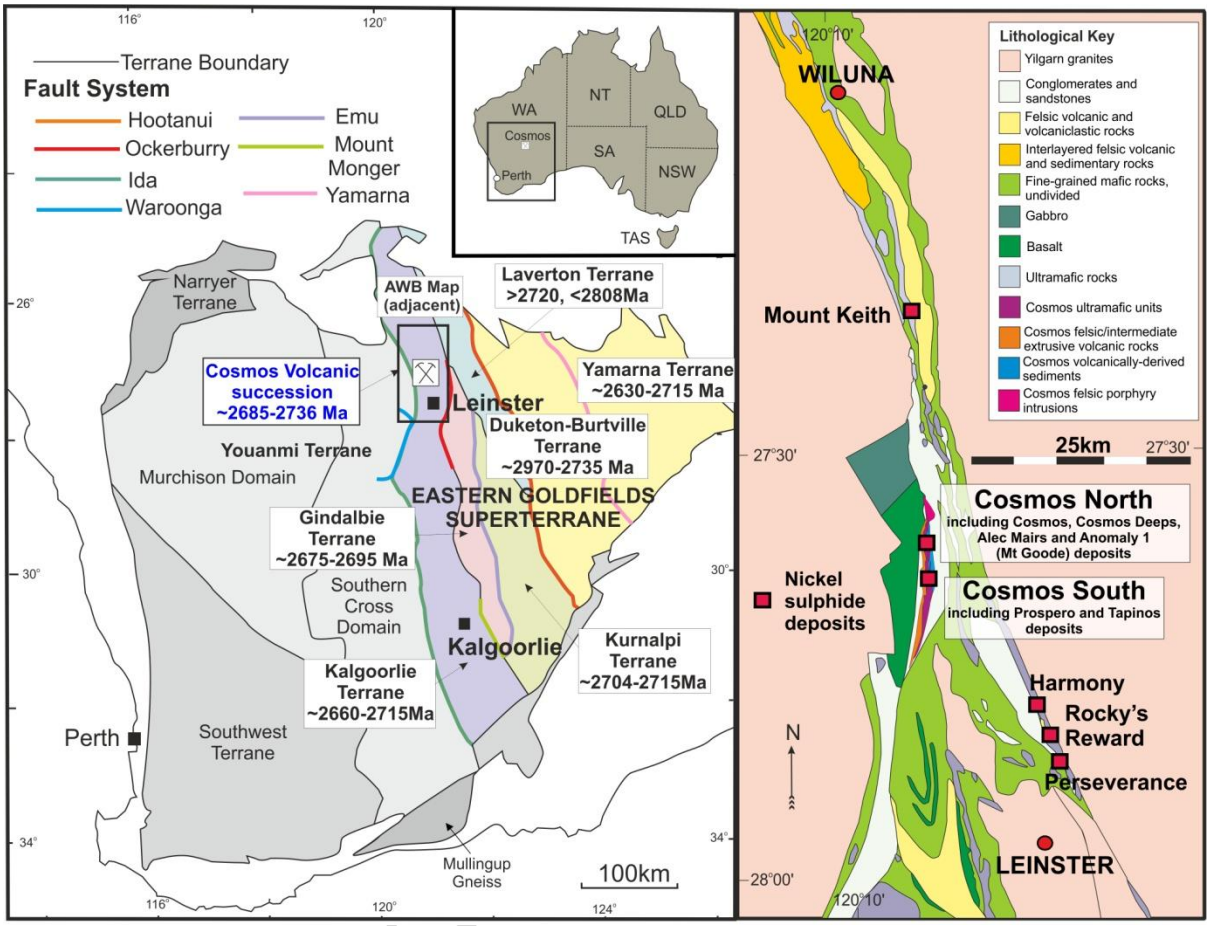

Figure 1

ACCEPTED

ACCEPTED MANUSCRIPT

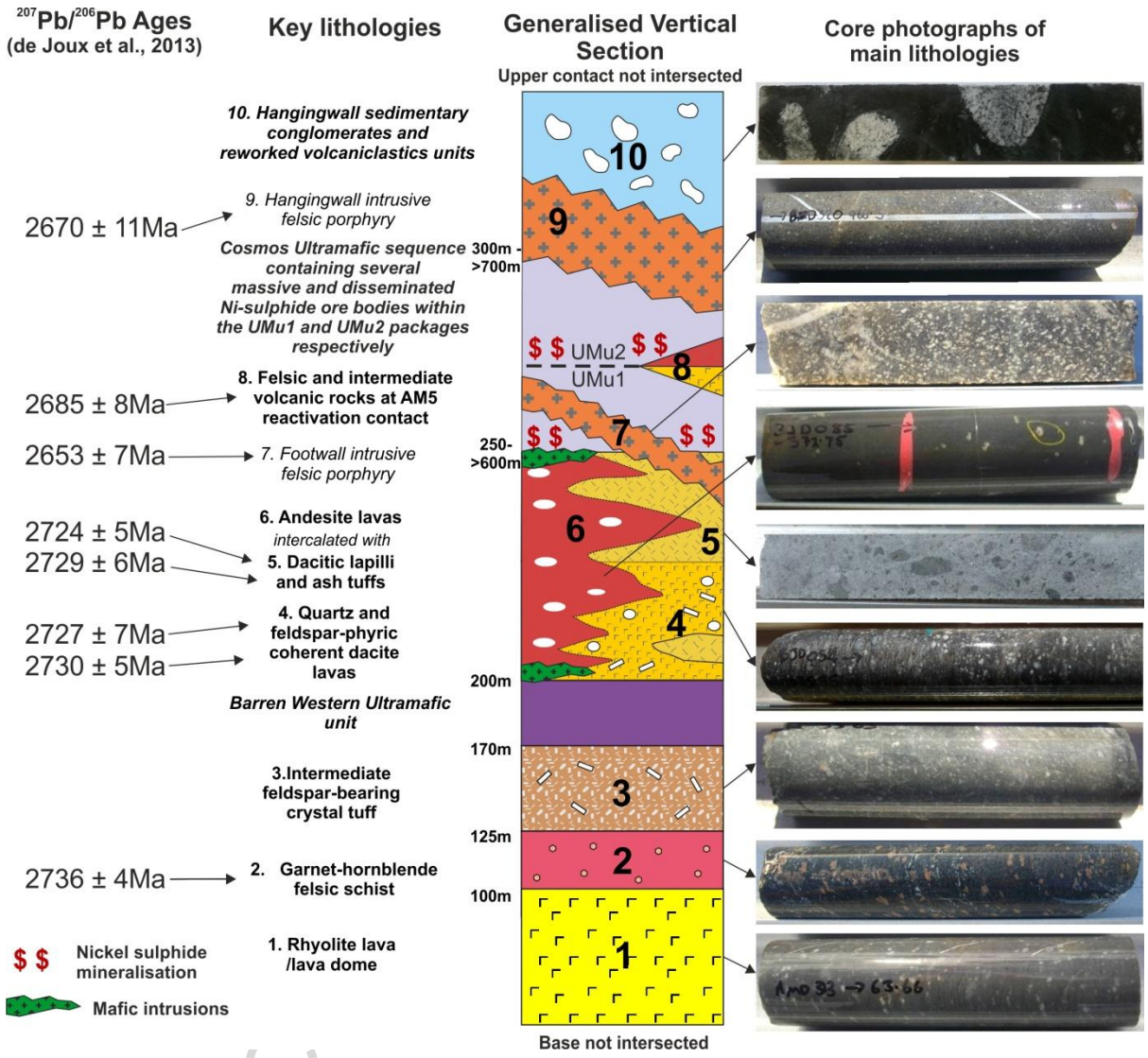

Figure 2

ACC

ACCEPTED MANUSCRIPT

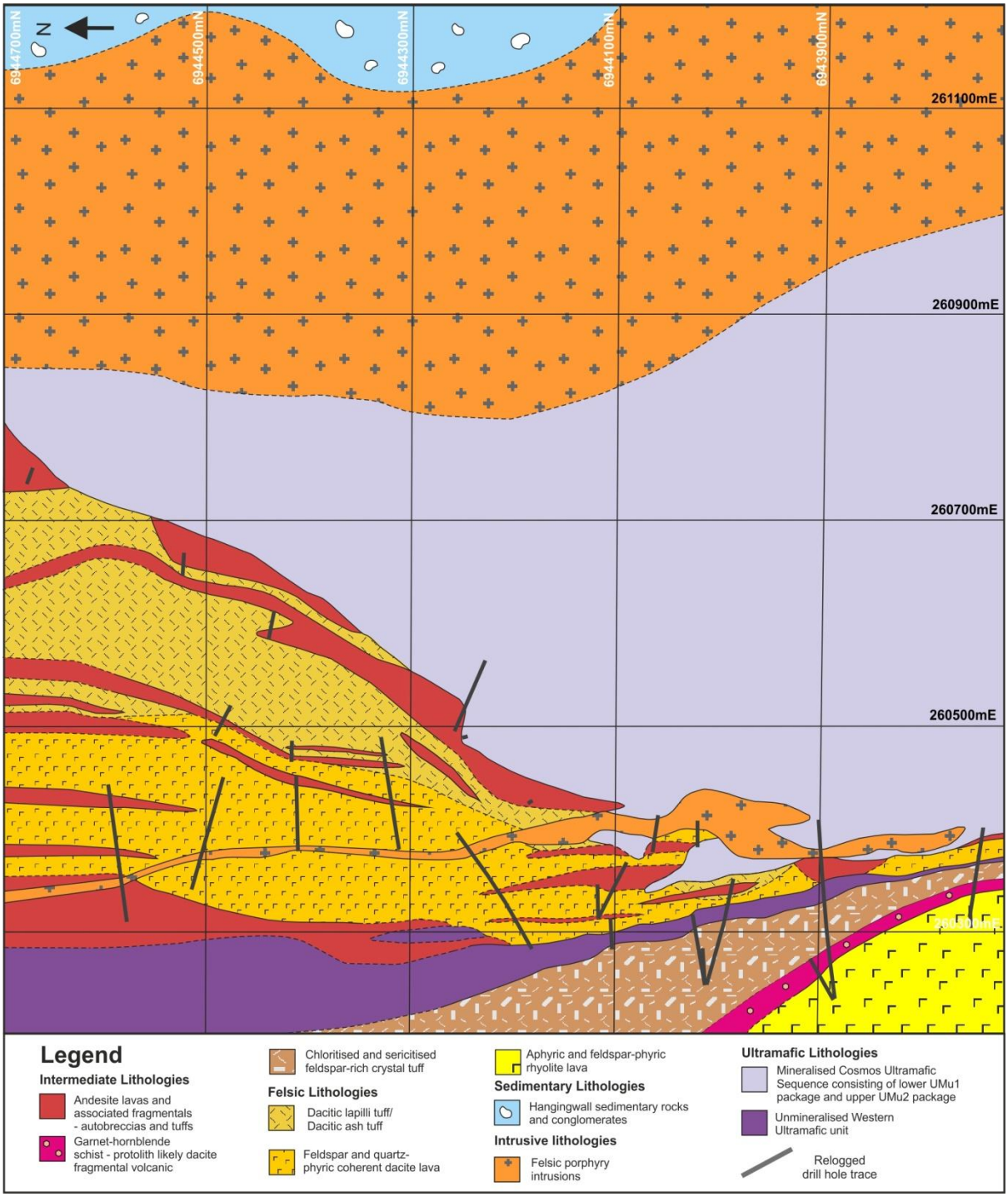

Figure 3

ACCEPTED MANUSCRIPT

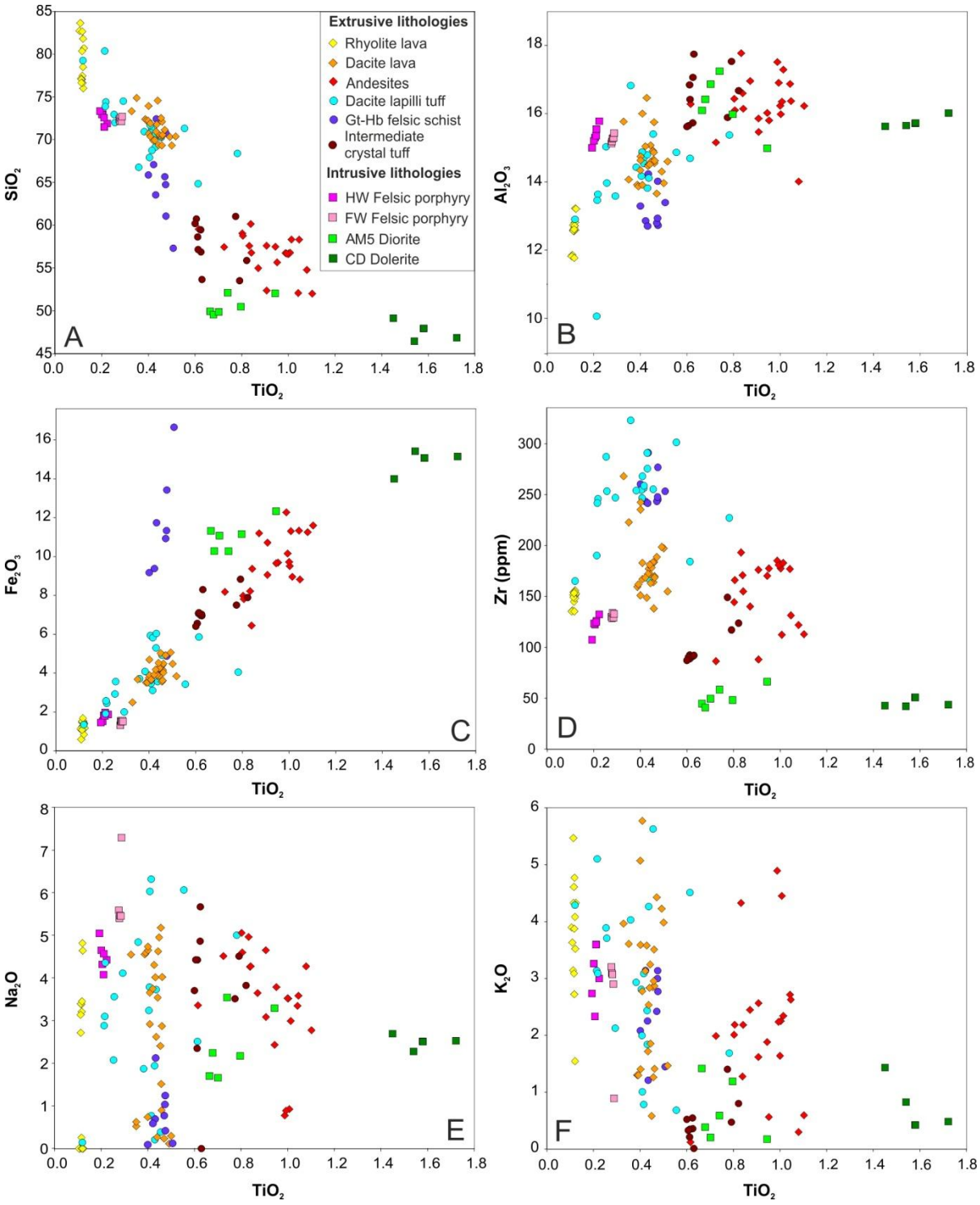

Figure 4

ACCEPTED MANUSCRIPT

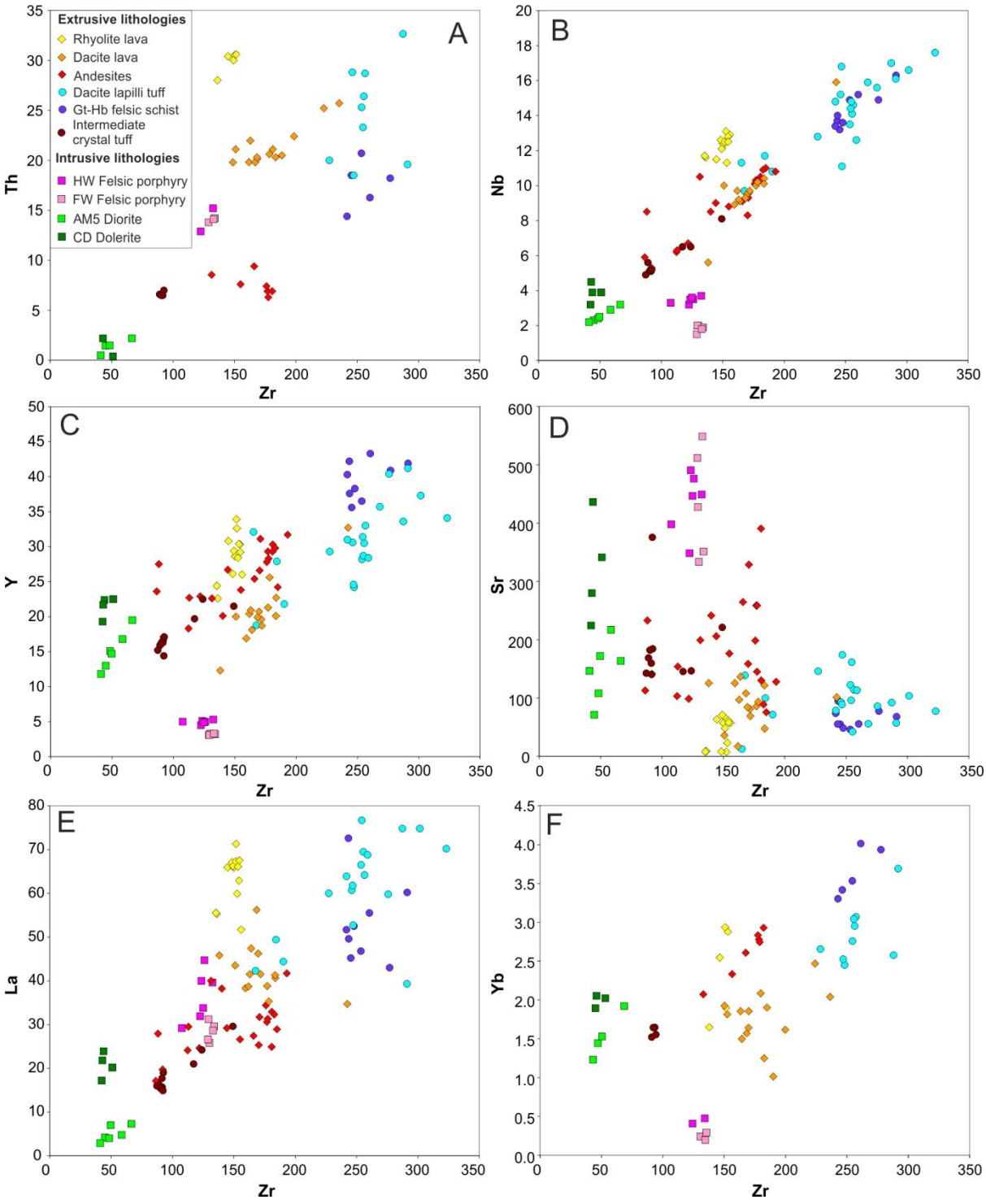

Figure 5

ACCEPTED MANUSCRIPT

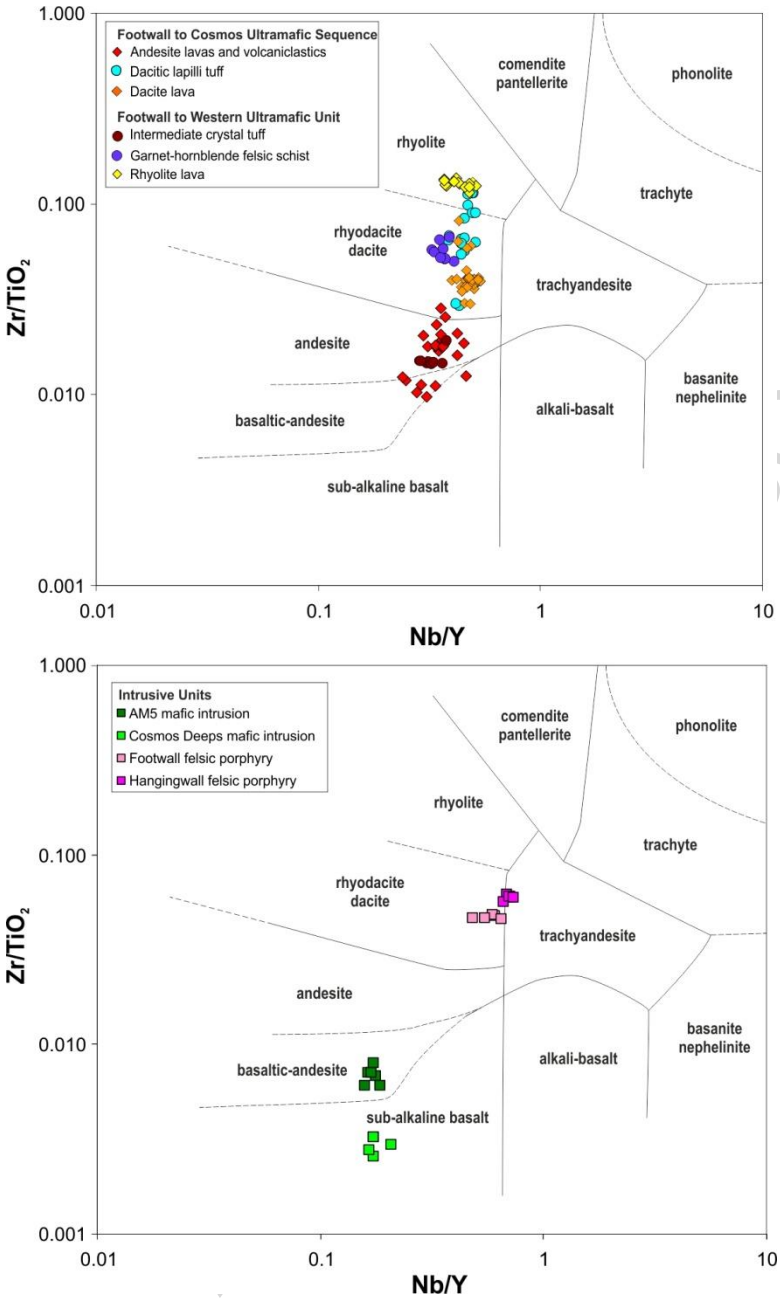

Figure 6

ACCEPTED MANUSCRIPT

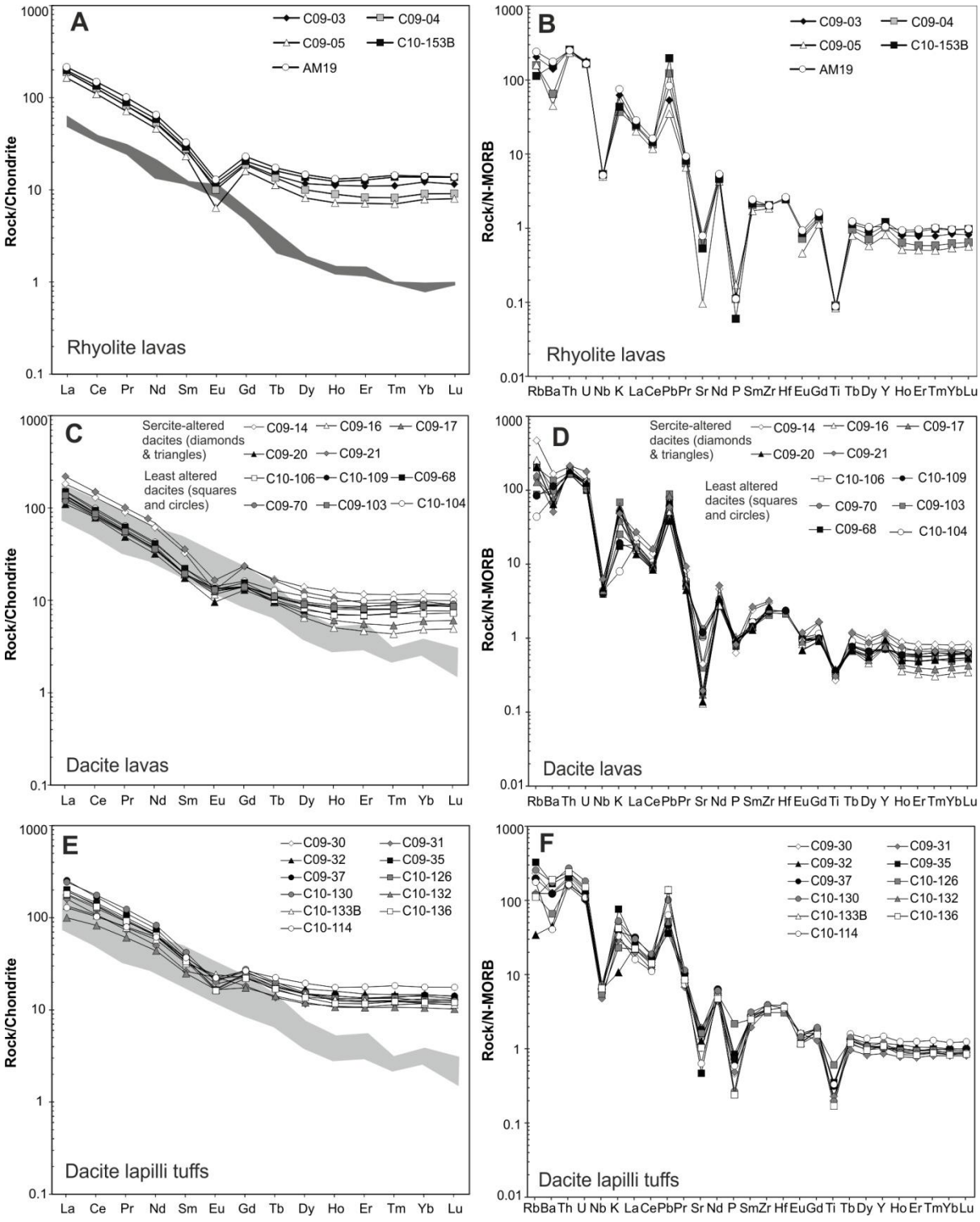

Figure 7a

ACCEPTED MANUSCRIPT

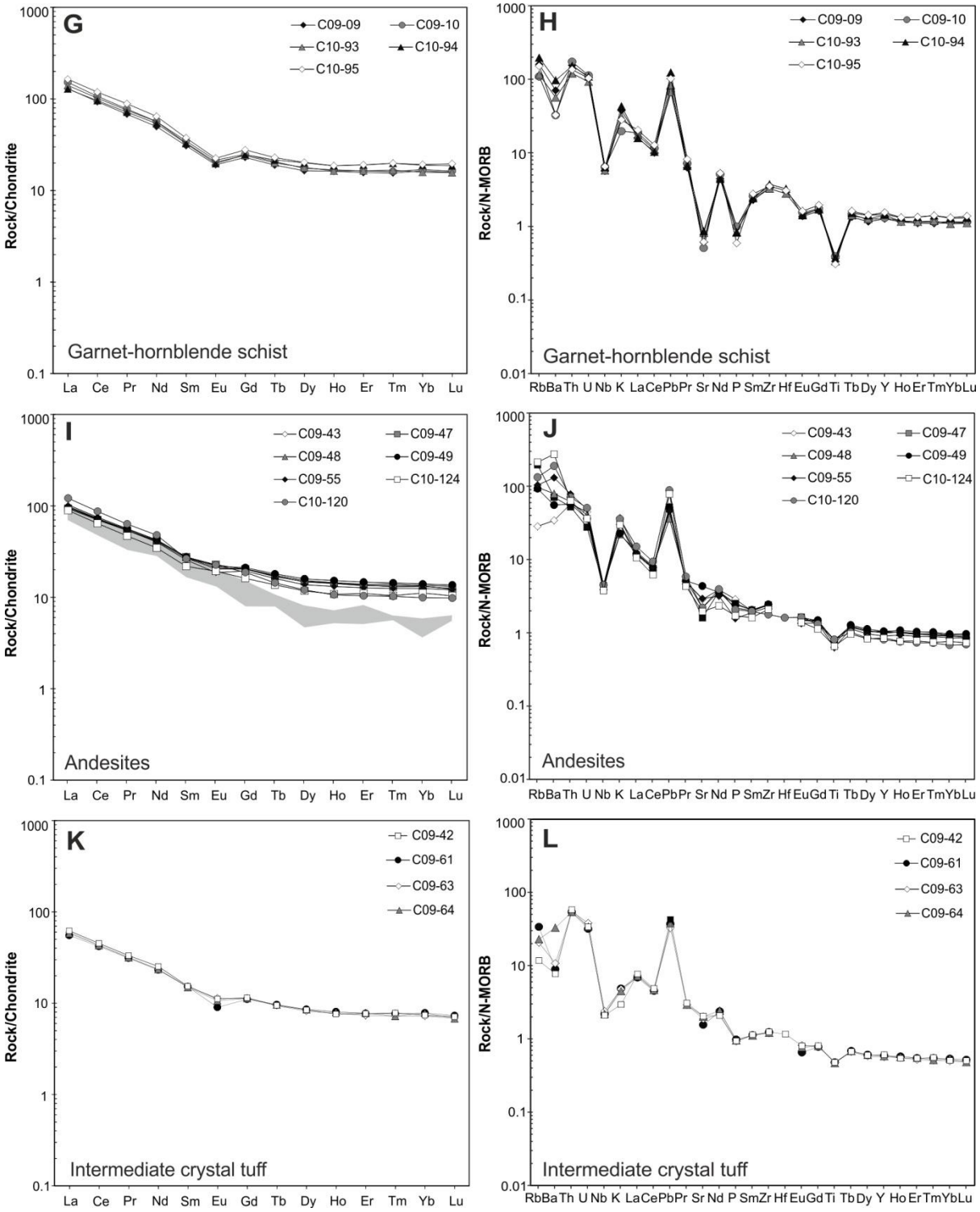

Figure 7b

ACCEPTED MANUSCRIPT

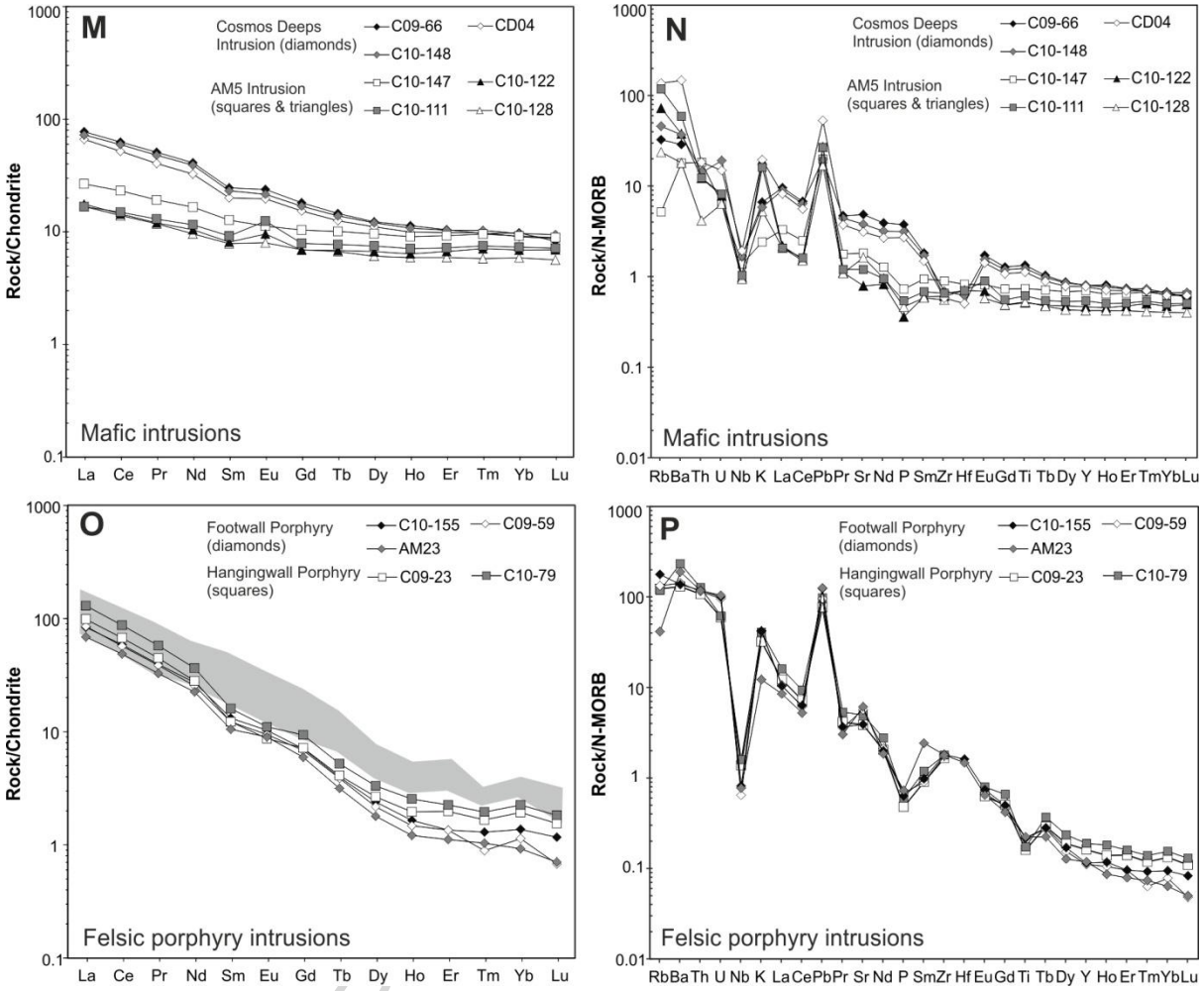

Figure 7c

ACCEPTED MANUSCRIPT

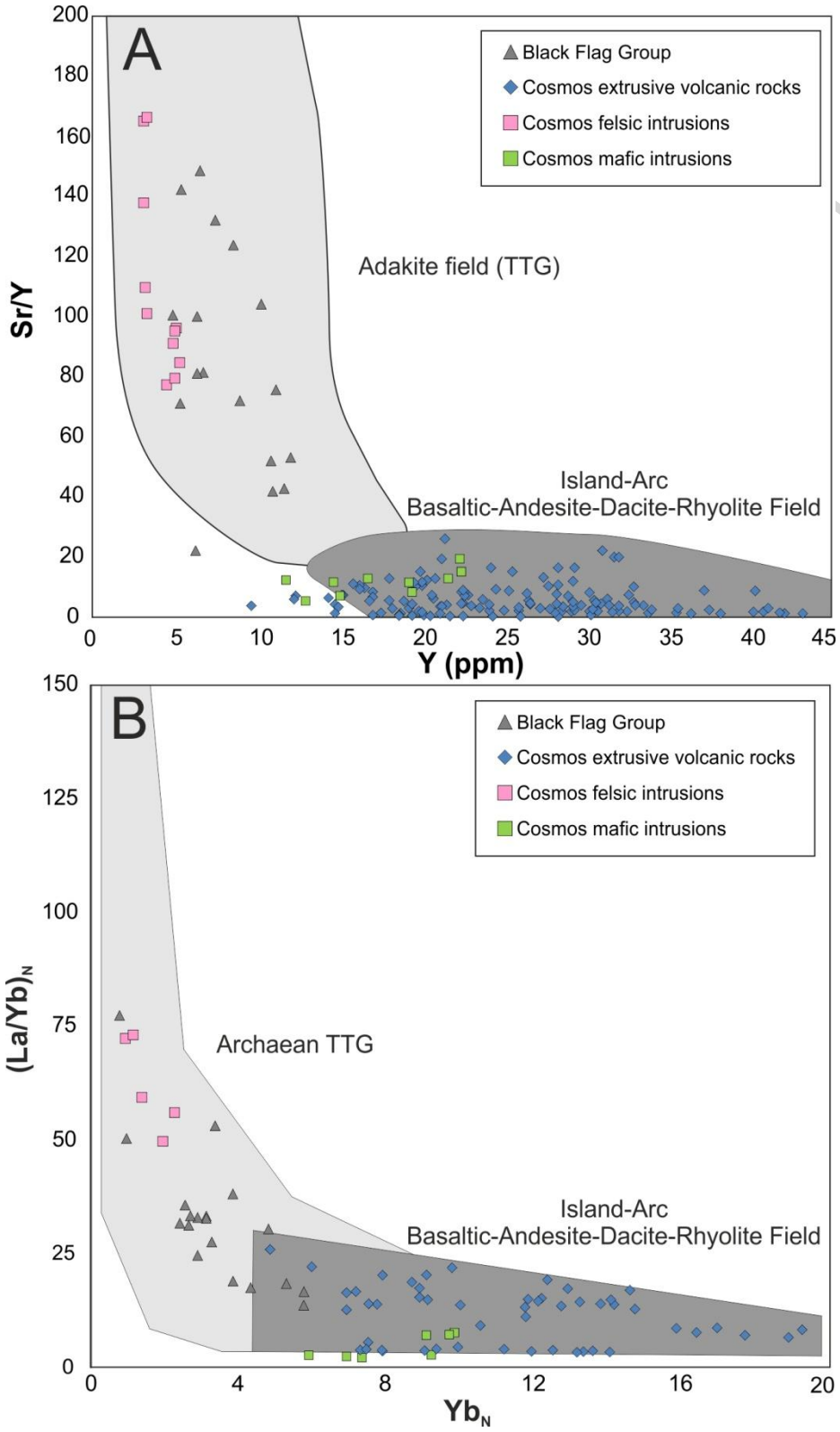

Figure 8

ACCEPTED MANUSCRIPT

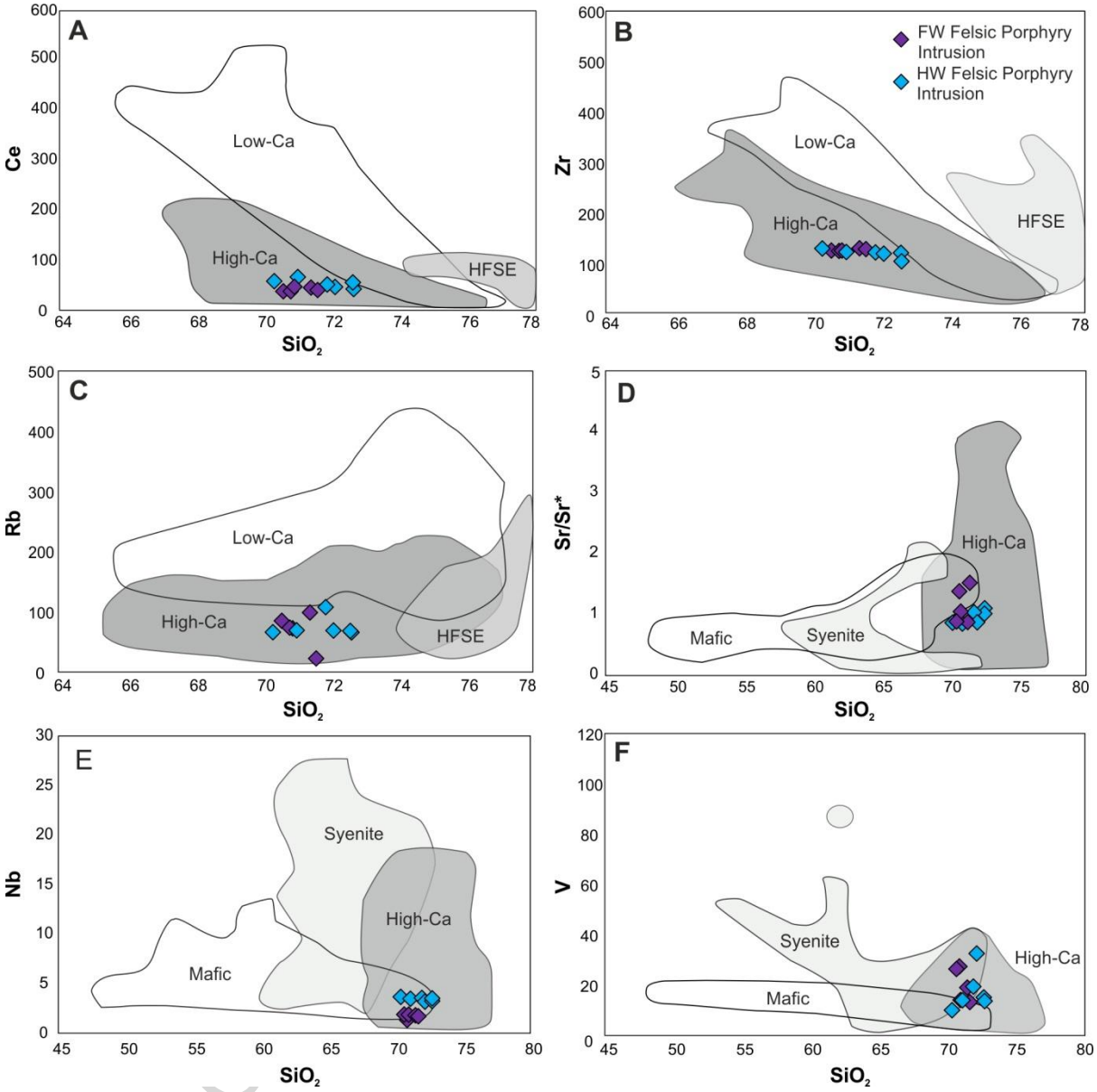

Figure 9

ACCEPTED MANUSCRIPT

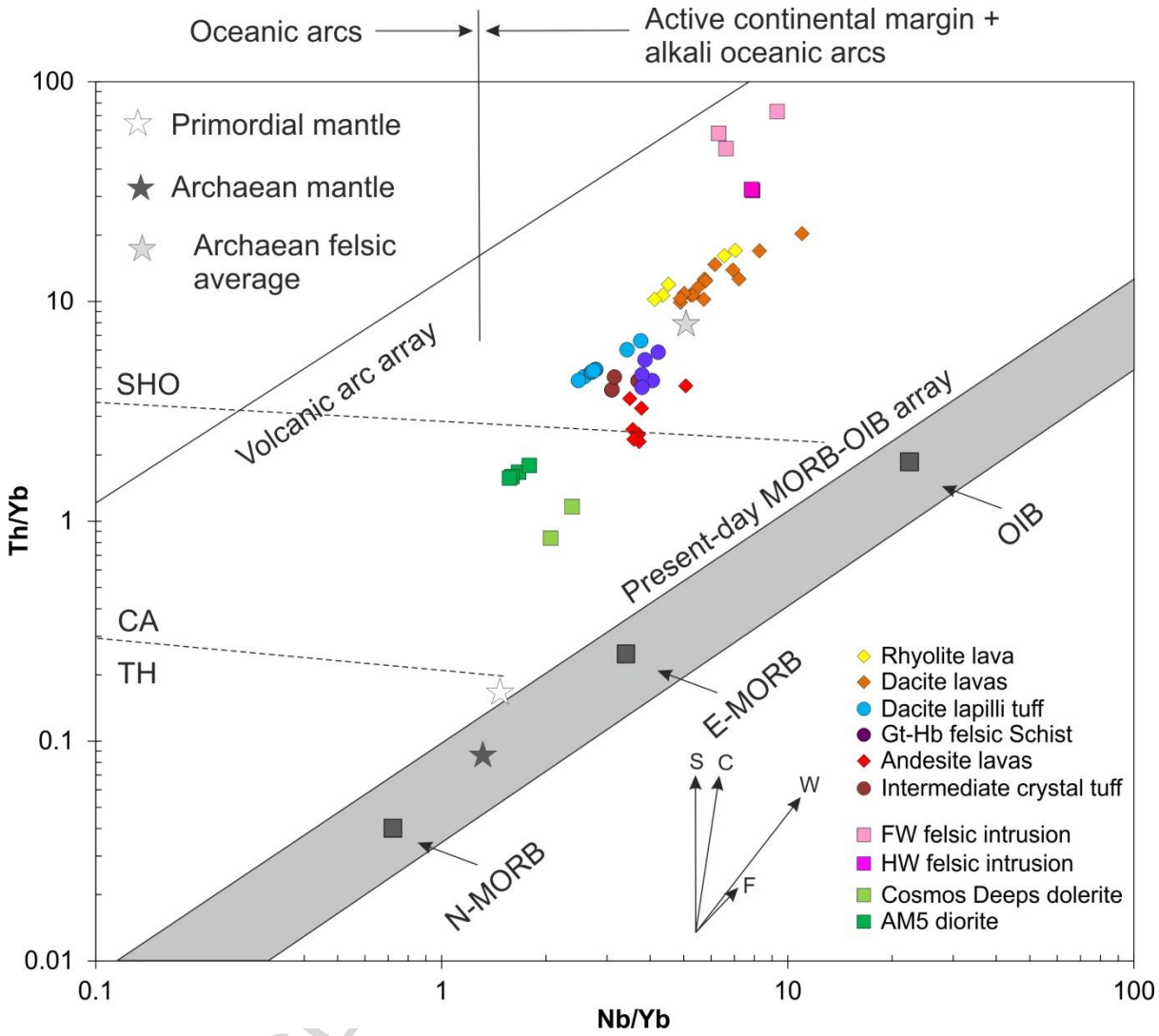

Figure 10

ACCEPTED MANUSCRIPT

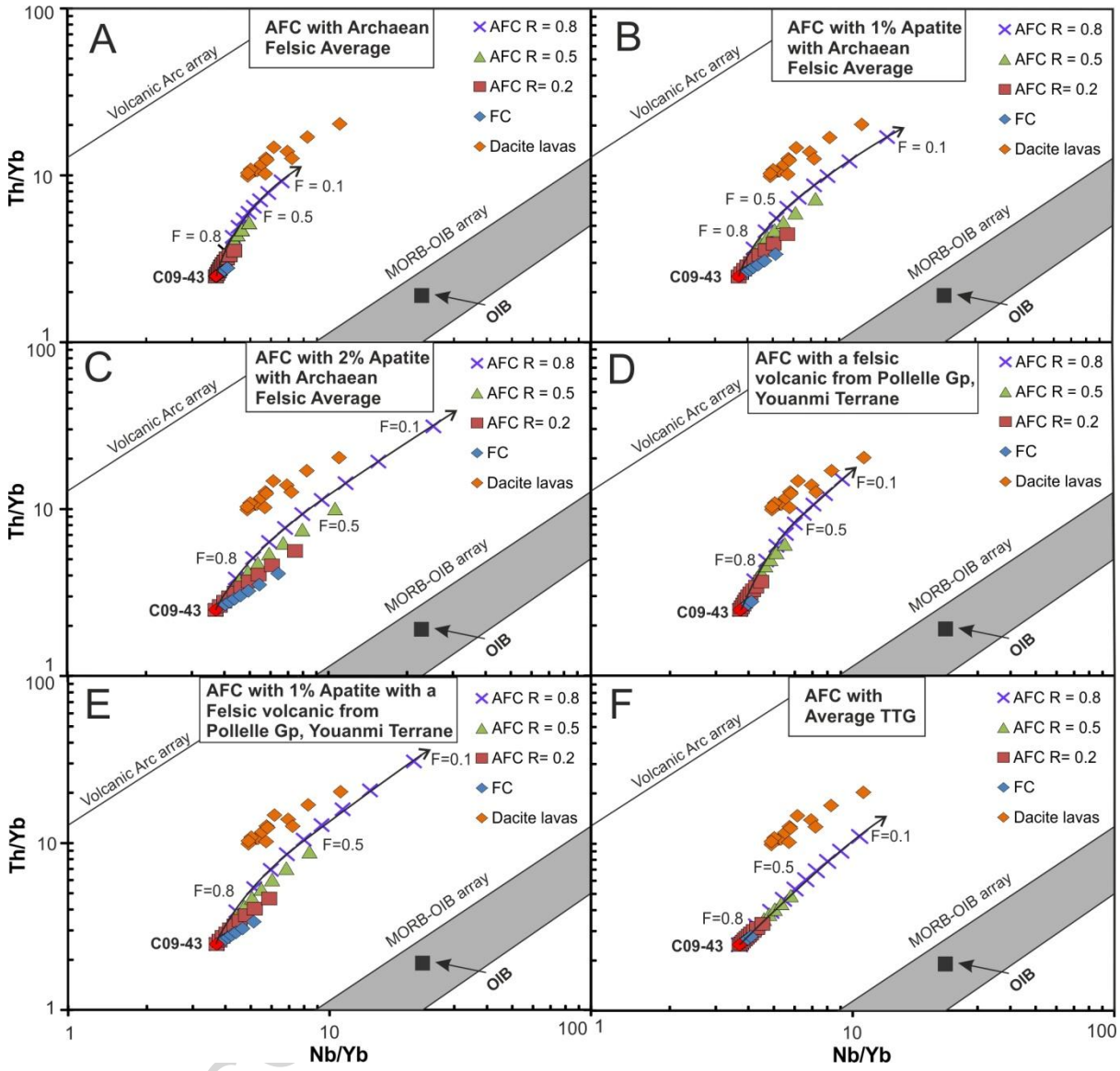

Figure 11

ACCEPTED MANUSCRIPT

Table 1 showing the age, mineralogy, volcanic facies and typical alteration styles of the main lithological groups within the Cosmos Succession.

Stratigraphic unit	Age	Mineralogy	Volcanic facies	Typical alteration type
Coherent rhyolite lava	> 2736Ma ± 4 Ma	Quartz + feldspar + sericite + biotite ± muscovite ± chlorite	Coherent porphyritic and aphyric rhyolite lava flow/dome. Feldspar phenocrysts in a cryptocrystalline quartz-feldspar groundmass	Sericitic
Garnet-hornblende felsic schist	2736Ma ± 4 Ma	Feldspar + garnet + hornblende + epidote ± chlorite	Recrystallised fragmental unit typified by skeletal porphyroblastic garnets in a hornblende and plagioclase-rich banded matrix. Occasional relic feldspar phenocryst fragments suggest the protolith is likely a crystal-rich felsic tuff	Sericitic
Intermediate feldspar-bearing crystal tuff	< 2736 ± 4 Ma	Feldspar + sericite + chlorite ± epidote	Andesitic crystal-rich tuff with abundant feldspar fragments and shards. Forms the immediate footwall unit to the Western Ultramafic unit	Sericitic, chloritic, epidote
Western Ultramafic unit	< 2736 ± 4 Ma, > 2730 ± 5 Ma	Lizardite + antigorite + tremolite actinolite + magnetite ± olivine	Barren olivine mesocumulates and orthocumulates that have been pervasively serpentinised and overprinted by metamorphic olivine, destroying primary cumulate and spinifex textures	Serpentinisation, metamorphic olivine
Coherent dacite lava	2730 - 2727 ± 7 Ma	Quartz + feldspar + sericite + biotite ± muscovite ± chlorite	Quartz and feldspar-phyric dacite lava package with occasional intermediate xenoliths. Embayed quartz phenocrysts common. Intercalated with andesite lavas and associated volcaniclastic horizons	Sericitic
Dacite lapilli tuff	2729 - 2724 ± 6 Ma	Quartz + feldspar + sericite + biotite ± muscovite ± chlorite	Dacite lapilli tuff with abundant relic feldspar phenocryst fragments and shards. Features tuff breccias with intermediate clasts. Intercalated with andesitic lavas and associated volcaniclastic horizons. Along with andesite lavas forms the footwall to the Cosmos Ultramafic Sequence	Sericitic
Andesite lavas and associated volcaniclastic horizons	2730 - 2724 ± 7 Ma	Feldspar + hornblende + biotite + chlorite ± quartz ± sericite	Variably amygdaloidal basaltic andesite to andesite lavas with autobreccias discernible in places. Associated volcaniclastic deposits. Intercalated with dacite lavas and lapilli tuffs. Along with dacitic tuffs forms the footwall to the Cosmos Ultramafic Sequence	Chloritic
Cosmos Ultramafic Sequence	< 2724 Ma	Lizardite + antigorite + tremolite actinolite + magnetite ± olivine ± chlorite ± Ni-sulphide	Dominantly olivine mesocumulates and olivine adcumulates and features spinifex-textured komatiites, olivine-pyroxene cumulates, olivine orthocumulates towards the unit's margin, although pervasive serpentinisation and overprinting by metamorphic olivine has destroyed primary volcanic textures. Contains numerous disseminated and massive high-tenor nickel sulphide ore bodies	Serpentinisation, metamorphic olivine
Stratigraphic unit	**Age**	**Mineralogy**	**Volcanic facies**	**Typical alteration type**
Mafic intrusions	<2724 Ma	Hornblende + feldspar + chlorite ± biotite	Two main mafic intrusions cross-cut the Cosmos volcanic succession at a shallow angle, notably the Cosmos Deeps Dolerite and the AM5 Diorite that both feature large distinct poikiloblasts of chlorite and hornblende	Chloritic
Hangingwall felsic porphyry intrusion	2670 ± 11 Ma	Quartz + feldspar + sericite + biotite ± muscovite ± epidote	Porphyritic felsic intrusion with small quartz and feldspar phenocrysts that crosscuts the upper contact of the Cosmos Ultramafic Sequence and the overlying hangingwall sedimentary package	Chloritic, epidote
Footwall felsic porphyry intrusion	2653 ± 7 Ma	Quartz + feldspar + sericite + biotite ± muscovite ± epidote	Porphyritic felsic intrusion with large feldspar phenocrysts that cross cuts the basal contact of the Cosmos Ultramafic Sequence	Chloritic, epidote

ACCEPTED MANUSCRIPT

Hangingwall sedimentary package	<2685 ± 8 Ma, >2670 Ma ± 11 Ma	Feldspar + amphibole + chlorite + biotite + quartz + sericite + muscovite + pyrite + garnet	Package of intercalated polymictic and monomictic conglomerates and reworked volcaniclastic sandstones and siltstones. Conglomerates feature granitic clasts in a more intermediate matrix	Chloritic

ACCEPTED MANUSCRIPT

ACCEPTED MANUSCRIPT

Table 2. Representative samples from the main lithological groups within the Cosmos succession. Major elements in wt. % and trace elements in ppm. n.d denotes below detection limit; – denotes not analysed. Trace elements reported to one decimal place were analysed by XRF, elements reported to two decimal places were analysed by ICP-MS. Gt-hb = garnet-hornblende.

Lithology	**Rhyolite lava**	**Felsic gt-hb Schist**	**Intermediate crystal tuff**	**Dacite lava**	**Strongly sericitised Dacite lava**	**Dacitic lapilli tuff**	**Andesite Lava**	**Hangingwall felsic intrusion**	**Footwall felsic intrusion**	**Cosmos Deeps mafic intrusion**	**AM5 mafic intrusion**
Sample name	**C09-03**	**C10-95**	**C09-61**	**C10-109**	**C09-17**	**C10-126**	**C09-48**	**CO9-23**	**C10-155**	**C10-148**	**C10-122**
SiO_2	75.43	64.20	55.40	69.47	73.52	67.35	57.11	72.13	71.42	47.47	49.03
Al_2O_3	12.29	12.95	16.62	14.39	14.83	15.14	15.72	15.12	15.03	15.56	15.80
Fe_2O_3	1.25	8.94	6.78	4.42	4.46	4.00	8.98	1.81	1.48	14.93	11.12
MnO	0.02	0.25	0.11	0.08	0.04	0.07	0.14	0.03	0.02	0.18	0.14
MgO	0.24	2.66	5.41	2.32	1.67	1.58	4.61	1.58	0.63	7.00	8.67
CaO	0.72	5.85	6.47	1.84	0.50	2.72	5.20	1.32	1.07	9.00	9.63
Na_2O	3.31	0.09	5.52	3.96	0.23	4.93	4.61	4.27	5.38	2.49	1.67
K_2O	4.52	2.03	0.35	1.39	2.80	1.66	1.61	2.31	3.02	0.42	1.40
TiO_2	0.11	0.39	0.61	0.45	0.43	0.77	0.90	0.20	0.28	1.56	0.65
P_2O_5	0.01	0.07	0.12	0.10	0.11	0.25	0.26	0.06	0.07	0.37	0.04
LOI	2.06	2.26	1.86	1.42	1.66	1.23	0.63	1.36	0.65	0.47	1.60
Total Majors	**99.96**	**99.70**	**99.24**	**99.85**	**100.25**	**99.69**	**99.76**	**100.18**	**99.06**	**99.46**	**99.75**
Zn	8.0	181.9	88.6	32.8	59.5	40.3	73.5	16.9	47.4	115.2	102.1
Cu	5.3	11.2	24.1	11.4	3.6	22.2	27.4	6.0	9.1	74.3	95.5
Ni	n.d	7.5	100.5	16.6	14.4	24.4	59.3	4.4	0.1	135.9	166.4
V	15.3	n.d	144.9	51.4	65.5	51.2	148.1	32.7	20.0	265.0	218.8
Ba	886.7	205.9	56.4	712.4	464.5	416.8	498.6	820.0	863.7	232.4	239.0
Sc	3.1	15.5	27.9	9.7	16.7	13.5	23.0	n.d	2.5	33.4	36.1
Nb	11.5	15.2	5.1	9.3	10.3	12.8	10.1	3.2	1.9	3.9	2.3
Zr	144.9	260.4	91.6	168.6	181.3	227.3	176.2	122.5	133.9	51.0	44.9
Y	30.8	43.3	16.6	19.9	21.6	29.3	27.8	4.5	3.2	22.5	13.0
Sr	63.1	55.5	140.4	107.8	15.6	145.9	198.3	348.2	351.1	341.3	71.1
Rb	114.6	84.7	19.0	47.4	72.5	65.5	54.3	68.8	99.4	25.7	40.7
Hf	-	6.3	-	4.8	-	6.3	-	-	3.3	1.3	1.5
U	8.4	4.9	1.5	5.5	5.5	5.2	1.9	2.8	4.7	0.9	0.4
Th	30.4	16.3	6.5	20.1	21.1	20.0	7.4	12.9	14.2	0.4	1.5
Pb	16.0	30.6	11.2	18.3	25.4	15.3	10.9	23.0	37.2	4.8	8.1
La	58.92	50.88	17.22	38.76	41.93	54.74	31.80	30.52	25.86	22.49	5.47
Ce	101.65	95.78	34.01	66.46	69.63	102.14	60.61	54.32	47.28	48.11	11.63
Pr	9.93	10.81	3.82	6.67	6.85	11.00	6.86	5.46	4.82	5.84	1.47
Nd	31.20	38.66	13.94	22.13	21.78	38.79	25.44	16.85	16.34	23.44	6.27
Sm	5.18	7.31	2.97	3.76	3.69	6.58	5.34	2.38	2.57	4.51	1.58
Eu	0.80	1.65	0.67	0.99	0.92	1.61	1.55	0.64	0.75	1.58	0.70
Gd	5.00	7.18	2.87	3.65	3.59	6.04	5.30	1.86	1.83	4.37	1.78
Tb	0.68	1.08	0.46	0.51	0.46	0.86	0.83	0.19	0.19	0.66	0.32
Dy	3.76	6.51	2.78	3.01	2.31	4.87	4.91	0.86	0.77	3.87	2.15
Ho	0.80	1.34	0.58	0.60	0.44	0.96	1.04	0.14	0.12	0.77	0.46
Er	2.31	4.00	1.63	1.78	1.17	2.78	2.91	0.42	0.28	2.17	1.41
Tm	0.36	0.64	0.25	0.29	0.17	0.43	0.45	0.05	0.04	0.33	0.23
Yb	2.54	4.01	1.64	1.85	1.24	2.65	2.83	0.40	0.29	2.02	1.44
Lu	0.37	0.63	0.24	0.29	0.19	0.40	0.42	0.05	0.04	0.30	0.22
Total Majors and Traces	**100.12**	**99.82**	**99.35**	**99.98**	**100.37**	**99.83**	**99.92**	**100.34**	**99.23**	**99.62**	**99.88**

ACCEPTED MANUSCRIPT

Table 3. Comparison of the geochemical attributes of typical TTG/D-affinity volcanic rocks with the average compositions of the Cosmos dacitic volcanic lavas, dacitic lapilli tuffs, felsic porphyry intrusions and the TTG/D-affinity Black Flag dacites (data from Morris and Witt, 1997).

	Typical TTG/D affinity rocks	**Average Cosmos dacite lavas**	**Average Cosmos dacite lapilli tuffs**	**Average Cosmos Hangingwall felsic intrusion**	**Average Cosmos Footwall felsic intrusion**	**Average Black Flag Dacite**
Al_2O_3 (wt. %)	**≥ 15**	14.34	14.22	15.87	14.98	16.00
Sr (ppm)	**300 - >2000**	88	102	463	434	635
Y(ppm)	**<18**	21	31	4.9	3.2	6.0
LREE	**Enriched**	Yes	Yes	Yes	Yes	Yes
HREE	**Depleted**	No	No	Yes	Yes	Yes
Eu Anomaly	**None or positive**	Negative	Negative	None	None	None
K_2O/Na_2O	**Commonly <1**	Highly variable due to mobility of alkaline phases	Highly variable due to mobility of alkaline phases	0.58	0.45	0.55

ACCEPTED MANUSCRIPT

Highlights

- We present a detailed geochemical investigation of the Cosmos greenstone succession
- The Cosmos sequence is considered to have formed in an ancient volcanic arc setting
- Volcanic lithologies have a distinct high-K calc-alkaline to shoshonite affinity
- Later intrusions have a TTG affinity and are related to regional granite intrusion
- Cosmos provides further evidence for plate tectonic operation in the Neoarchaean

ACCEPTED MANUSCRIPT